Electrical Properties of Iron-Doped Silicon at Different Stages of Precipitation

Dissertation
zur Erlangung des Doktorgrades
der Mathematisch-Naturwissenschaftlichen Fakultäten
der Georg-August-Universität zu Göttingen

vorgelegt von
Reda Mahsoop El Naby Mohamed Baiomy Khalil
aus
Kalubia | Ägypten

Göttingen 2004

D 7

Referent: Herr Prof. W. Schröter

Koreferent: Herr Prof. H. C. Freyhardt

Tag der mündlichen Prüfung: 29.11.2004

Contents

Chapter 1

Introduction

Solid-state electronics was introduced with the experimental discovery of voltage and power gain in a point-contact transistor by Bardeen and Brattain at Bell Laboratories on December 16, 1947[1]. The extensive investigation and development in solid-state electronics led to the invitation of the ”solid circuit”, which was eventually judged by the courts to be the first semiconductor integrated circuit (IC)[2]. Since the creation of the first IC, the density and complexity of electronic circuits manufactured on a semiconductor chip have been increased from small-scale integration, to medium-scale integration, to large scale integration, to very large scale integration, and finally to ultra-large-scale integration, which consists of 10^7 or more components per chip. The increasing component density has been achieved by shrinking the feature size, which is smaller than 1 μm for ULSI circuits. This shrinking requires higher yields and hence a decreasing density of defects in the electrically active zone of a device.

The major electronic material today is the crystalline silicon. Although other materials have parameters superior to those of silicon for many important applications, they have not displaced silicon in commercial devices. Unintentional impurity contamination of clean silicon wafers is still a serious problem. There are many kinds of likely impurity contaminations and contamination sources during the manufacturing of silicon devices. Oxygen, carbon and transition metals are incorporated into silicon crystal during device fabrication as well as during crystal growth and wafer shaping processes. These impurities play a very special role in generation of process-induced defects. Transition metal impurities represent an interesting system for defect studies. These impurities can occupy both the substitutional and tetrahedral interstitial lattice sites and they introduce deep levels in the band gap.

Iron, copper, nickel and cobalt are the most common impurities in silicon device fabrication. The precipitates of copper are known to reduce the lifetime of the electronic device[3]. Copper[4] and nickel[5] cause a breakdown in the silicon oxides. Iron-boron pairs have been found to have a detrimental effect on solar cell efficiency in concentration around 10^{13}cm^{-3}[6, 7], and even in the 10^{11}cm^{-3}[8] range.

Iron in silicon has been intensively studied during the past three decades by experimentalists as well as theoreticians. The topic is of considerable interest to the semiconductor industry as iron is incorporated inevitably into silicon during the growing of silicon and processing of electronic devices. Sources of iron introduction include several cleaning and etching procedures and high temperature treatments. Iron is a fast diffusing species that readily interacts with other defects in the crystal, including vacancies, self-interstitials, dopants, oxygen and other transition metal.

A hot topic in the field is the electrical activity of several iron-related defects in silicon, in particular iron-clusters and iron silicide precipitates. Yet, many issues remain unresolved. Reviews on iron in silicon have been given by Istratov et al.[9, 10].

The aim of this Thesis is to precipitate the iron and to study the electrical properties of the interstitial iron-clusters and iron-precipitates in p-type silicon. Our experimental technique is the Deep-Level Transient spectroscopy (DLTS). The Thesis is divided into five chapters. In Chapter 2, we describe aspects of the physical properties of the iron in p-type silicon and introduce the concept of deep centres and their electrical activity for iron interstitial, cluster and precipitate. Further, an introduction to point defect and extended defect models is given, which form the foundation for the interpretation of capacitance-transient measurements. In Chapter 3, various experimental preparation procedures and techniques used for characterization of defects in semiconductors are presented. In Chapter 4, we consider the precipitation of iron in p-type silicon for different low-temperature annealing treatments and iron concentration. The total amount and the form of iron introduced under various experimental conditions are quantified by DLTS. In addition, we present the observation of capacitance changes with iron cluster and precipitates to those related to majority carrier emission from extended states in the band gap, which are related to iron-clusters and iron precipitates. In Chapter 5, we discuss the electrical properties and the electronic structure of iron-cluster and iron-precipitate. The electrical properties of iron precipitates are analyzed in detail and it is concluded that iron-cluster and iron-precipitate defects are associated to localized and bandlike states, respectively. Finally, the Thesis is summarized.

Chapter 2

General considerations

2.1 The physical properties of iron in silicon

Iron is certainly one of the most troubling contaminants in silicon materials for solar cell and electronic applications because the iron is a common element in nature and is difficult to completely eliminate in a production line. Therefore, the unintentional iron contamination level in wafers is usually higher than that of other metal impurities[11].

The major reasons why transition metals in general, and iron in particular, are detrimental for silicon devices are; first transition metals as well as their complexes and precipitates introduce deep levels into the band gap, reducing the minority carrier lifetime or generating minority carriers in depleted regions. Second, the incorporation of metals into gate oxides or their precipitation at Si/SiO_2 interfaces degrades MOS device yield[12, 13]. Third, very high diffusion coefficients at high processing temperatures can result in fast contamination of large wafer areas even from point sources and from the wafer backside.

Understanding the electrical properties of extended defects like dislocations, grain boundaries and precipitates is important for semiconductor technology. Interaction with point defects/impurities can largely change the properties of such defects, so the influence of technologically steps on defect activity is of particular interest.

The transition metals show exponentially decreasing solubility in silicon with the temperature[14]. Quenching a crystal, which has been saturated at the diffusion temperature, to room temperature results in a supersaturation which is large compared with that usually attainable in metallic solutions. This corresponds to a driving chemical potential for precipitation at room temperature approximately 1 eV per atom. By rapid quenching it is possible to keep the iron with their major part in solution, while copper and nickel precipitate during or immediately after quenching[15]. For nickel and copper the diffusion constant at high temperatures is about one and two order of magnitude larger than that of iron, so that precipitation even near room temperature could be possible.

Iron precipitates in the first stage (iron-cluster) during the storage at room temperature or at low annealing temperature (120 - 140°C), which was detected only by EPR. In addition, iron precipitates in stable slicide phases, which are α- and $\beta-\mathrm{FeSi}_2$ above and below 915°C, respectively.

Until now, little work has examined how iron precipitates in bulk. What are the electronic properties, morphology and composition of the first particles. What are the mechanisms which make them grew? By means of DLTS, we have studied the iron in p-type silicon to obtain the answers to these questions.

The interrelation between the electrical properties, formation and atomic structure of iron-cluster and iron-silicide precipitates has been described in iron doped FZ p-type silicon. After rapid quenching and subsequent annealing, iron gives rise to iron interstitial and\or extended defect states (iron-clusters and iron-precipitates) depends on the annealing temperature and iron concentration. For interstitial iron-clusters, deep localized states have been attributed to more than four iron atoms bounding the iron-clusters and iron-precipitates, deep bandlike states have been attributed to the $\gamma - \mathrm{FeSi}_2$.

Compared to nickel, however, much less is known about the atomic structure of iron-cluster and iron-precipitate. While providing a coherent picture of precipitates growth, ripening and electronic structure, the questions how the clusters nucleate and whether structurally different precursor stages exist, are open.

2.1.1 Iron interstitial

The analysis of the physics of iron as an impurity in silicon demonstrated[14], that iron dissolves and diffuses in silicon in the interstitial state. If an iron contaminated wafer is cooled down rapidly, all iron will be quenched on interstitial sites and will form a deep level at $(E_\mathrm{V} + 0.38)$ eV. However, since $\mathrm{Fe_i}$ is mobile and can diffuse short distances in the wafer at room temperature (its diffusion coefficient at 300°C is approximately $3 \times 10^{-15}\mathrm{cm}^2/\mathrm{s}$), it quickly forms pairs with shallow acceptors, for example boron. The binding energy is the electrostatic attraction between positively charged (in p-type at room temperature) interstitial iron and negatively charged boron. FeB pairs form a donor level at $(E_\mathrm{V} + 0.1)$ eV and an acceptor level at $(E_\mathrm{C} - 0.26 \pm 0.03)$ eV[16]. Although FeB pairs are stable at room temperature, they can be easily dissociated by annealing the sample at 200°C or by shining white light on the wafer. The reactions of formation and dissociation of FeB pairs, which reversibly change the electrical levels associated with iron and its recombination activity, is one major fingerprint of interstitial iron in silicon.

Besides complexes with shallow acceptors (B, Al, Ga, In, Ti)[17, 18, 19, 20] interstitial iron is known to form electrically active complexes with gold[21], silver, zinc[22], platinum, palladium[23], sulphur[24] and oxygen[25]. These complexes altogether form about 20 energy levels in the silicon band gap.

2.1.2 Iron cluster

Iron-cluster defects were observed in electron-irradiated iron-doped samples by using Electron-Paramagnetic-Resonance (EPR)[26]. The previous authors concluded that these defects contain iron and irradiation-induced defects, most probably, vacancies. This defect consisted of two iron atoms and was tentatively identified as $(\mathrm{Fe_iFe_iV})^-$, $(\mathrm{Fe_iFe_iV_2})$ or $(\mathrm{Fe_iFe_iV})^+$. In addition, the cluster, which consistes of four atoms, was formed at annealing above 120°C. However, Ammerlaan[27] changed the designation of the $(\mathrm{Fe_iFe_iV})^+$ spectrum to belong to the $\mathrm{Fe_iFe_i}$ complex. The EPR spectrum of $\mathrm{Fe_iFe_i}$ pairs was identified by Muller et al.[26] above and further studied by J. van Kooten et al.[28] and Gehlhoff et al.[29]. It was found[28] above that this complex can be observed in quenched non-irradiated samples, thus indicating that the complex does not contain irradiation-induced defects (vacancies or self-interstitials).

J.J. van Kooten et al. reported that these defects formed after the quench and disappeared after a storage at room temperature for 12 h, or after an anneal at 75°C for 1 h. They concluded that the disappearance of this defect at or just above room temperature indicates that there is a strong preference for the further aggregation of iron at this defect.

2.1.3 Iron silicide

The study of the formation of iron precipitates in silicon has attracted a considerable amount of attention for its potential in Si-based optoelectronic, integrated circuits and solar cell applications.

Bulk precipitation of transition metals in the form of the metal-silicide is thoroughly investigated for fast diffusing metals such as copper and nickel[30, 31]. Similar to other transition metals, iron forms a number of silicide phases, including cubic ε-FeSi, tetragonal α-$\mathrm{FeSi_2}$, orthorhombic β-$\mathrm{FeSi_2}$, hexagonal $\mathrm{Fe_5Si_3}$ and cubic $\mathrm{Fe_3Si}$[32, 33]. Note that it is usually much more difficult to find iron-silicide precipitates in the bulk of a silicon wafer after thermal diffusion and cool down, than to find precipitates of copper or nickel. This is because the solubility of iron (around 10^{16} cm^{-3} at 1200°C, or around 3×10^{12} cm^{-3} at 800°C) is much lower than that of copper or nickel and the resulting density of precipitates, if they are formed in the bulk, is low. Additionally, it is very difficult to observe the precipitates in the bulk by using Transmission Electron Microscopy (TEM) because the strain fields around the precipitates are low. Furthermore, the pairing of iron with boron is an efficient trapping mechanism, which significantly reduces the driving force for the precipitation of iron in the bulk. Several groups[34, 35, 36, 37] succeeded in finding rod-like $FeSi_2$ precipitates, up to 0.5 μm long and a few tenths of a nanometer thick, in TEM samples prepared from devices or wafers after thermal in-diffusion of iron. These iron-silicide precipitates were found at Si/SiO_2 interfaces. The most observations of iron-precipitates were done after implantation of high doses of iron (which results in extremely high locale concentrations of iron) with subsequent annealing[12, 38, 39, 40].

It has been observed experimentally that iron does not precipitate during cooling of defect-free silicon[36]. Thus lattice defects and other impurity precipitates serving as nucleation sites strongly enhance iron precipitation. From TEM investigations it was deduced that iron precipitates as α-$FeSi_2$ in the form of rod-like defects[41] or as β-$FeSi_2$ during subsequent annealing processes[42]. Precipitates grew during a moderately-fast cooling of the sample from high temperature. In some cases, iron precipitates have exhibited additional small precipitates. These small crystalline particles resemble precipitates of copper silicide, which may have formed the nuclei for the iron precipitation.

A number of researchers tried to detect the iron precipitation using capacitance spectroscopy methods (DLTS) or Surface Photo-Voltage (SPV). Mesli et al.[43] applied the DLTS technique to investigate the kinetics of interstitial iron precipitation in p-type silicon corresponding to the charge of the iron atom. Indeed, the iron charge state is controlled by the applied reverse voltage during the annealing. They concluded from their observation that iron in the neutral charge state precipitates preferentially in three-dimensional nucleation centres while iron in the positive charge vanishes in the dislocation line. Additionally, these centres are created during the fast cooling procedure necessary to dissolve iron in the silicon matrix.

W. B. Henley and D. A. Ramappa[44] have experimentally investigated temperature dependent iron precipitation in FZ-Si. Iron precipitates was introduced in silicon over a wide thermal process temperature range and time and analyzed by a quantitative assessment of change in interstitial iron using SPV. It was concluded that maximum iron precipitation occurs in the temperature range of 500-600°C with iron concentration in the range $10^{11} - 10^{13}$ cm^{-3}.

2.2 The principle of DLTS technique

Capacitance measurements are widely used to study the emission and capture of holes and electrons at deep traps in semiconductors. These methods use the principle, that the high-frequency capacitance of the depletion region of a diode or p-n junction is related to the distribution of the space charge in the region, so that a change in the electronic occupancy of a trap will result in a change in capacitance.

DLTS was introduced in 1974 by Lang[45, 46], and quickly became an important technique for the detection and identification of impurities in semiconductors and the investigation of defect reactions. Deep level traps are detected by DLTS in a thin (about 0.5 to 3 μm) near surface depletion layer formed by a reverse biased Schottky diode or a p-n junction.

As the applied bias voltage is rapidly increased, the majority charge carriers will quickly (typically within less than 10^{-10}s) drift out of the depletion region, leaving the ionized shallow donors/acceptors behind. The charge carriers trapped by the impurities will also eventually leave the depletion region after they are thermally emitted to the conduction (in n-Si) or valence (in p-type) band. The emission process, however, is much slower than the drift of free charge carriers, and can be observed by monitoring changes in the capacitance of the diode.

In a DLTS experiment[45] above the occupation of a deep trap is transiently increased by a filling pulse caused by abrupt changes in the reverse voltage, which is applied at the diode sample structure. The relaxation to equilibrium occurs via the emission of excess charge carriers (in this case electrons) which can be monitored by a corresponding capacitance transient $C(t,T)$. In the simplest case, $C(t,T)$ exhibits an exponential character with

$$C(t,T) = C_o - \Delta C \exp(-e_{\mathrm{p}}t) \tag{2.1}$$

Here C_o denotes the equilibrium capacitance value at reverse bias voltage and ΔC the lowering of C_o directly after the filling pulse ($t = 0$).
The change in capacitance, $\Delta C(t) = C(t) - C_o$, is proportional to the density of traps, N_{T}, and inversely proportional to the doping concentration, N_{D}, as $2\Delta C/C_o \sim N_{\mathrm{T}}/N_{\mathrm{D}}$. The sensitivity of DLTS is usually in the range of $N_{\mathrm{T}}/N_{\mathrm{D}} \approx (10^{-5}$ to $10^{-6})$.

Analysis of the exponential transients taken as a function of temperature gives the activation energy (thermal enthalpy) for the emission of charge carriers from the trap to conduction or valence band, majority carrier capture cross-section of the trap and the trap concentration. By varying the bias voltage U_{B}, filling pulse duration t_{p} and amplitude of the pulses U_{p}, one can study depth distribution of the traps in the depletion region, distinguish donor and acceptor traps, and also between point and extended defects[47].

2.3 The modelling of DLTS

2.3.1 Point defect

The occupation of a level in the upper half of the gap (n-type) is determined by capture and emission by electrons from the conduction band. The occupation degree, f, of the level is given to by the ratio of the density of the levels n_{T}^{-} occupied with an electron and the total density N_{T}, $f = \frac{n_{\mathrm{T}}^{-}}{N_{\mathrm{T}}}$.
For the simplest case of a point defect the following rate equation describes the time-dependent change of occupation of the defect:

$$\frac{\partial f}{\partial t} = c_{\mathrm{n}} n(1-f) - e_{\mathrm{n}} f \tag{2.2}$$

$c_{\mathrm{n}} n$ is the capture rate and e_{n} is the emission rate of the electrons. The free charge carrier density, n, in the neutral semiconductor is given by

$$n = N_{\mathrm{C}} \exp\left(-\frac{E_{\mathrm{C}} - E_{\mathrm{F}}}{k_{\mathrm{B}} T}\right) \tag{2.3}$$

where N_{C} is the effective density of states in the conduction band. In thermodynamic equilibrium the occupation degree does not change ($df/dt = 0$). For the occupation degree in the equilibrium f_{eq} arises therefore:

$$f_{\mathrm{eq}} = \frac{1}{\left[1 + \frac{e_{\mathrm{n}}}{c_{\mathrm{n}} n}\right]} \tag{2.4}$$

On the other hand the occupation of a level is given by the Fermi distribution in the thermodynamic equilibrium:

$$f_{\mathrm{eq}} = \frac{1}{\left[1 + \exp\left(\frac{E_{\mathrm{T}} - E_{\mathrm{F}}}{k_{\mathrm{B}} T}\right)\right]} \tag{2.5}$$

whereby E_{T} represent the energy level and E_{F} the Fermi energy. From equations 2.3, 2.4 and 2.5 one receives the expression for the emission rate:

$$e_{\mathrm{n}}(T) = c_{\mathrm{n}} N_{\mathrm{C}} \exp\left(-\frac{E_{\mathrm{C}} - E_{\mathrm{T}}}{k_{\mathrm{B}} T}\right) \tag{2.6}$$

The chemical potential is defined as the increase in Gibbs free energy, G, per electron-hole pair or carrier-ionized defect pair at constant temperature. Following these definitions Engström and Alm[48] have suggested that the rate of thermal emission of carriers from a deep state at temperature T is

$$e_{\mathrm{n}}(T) = \sigma_{\mathrm{n}} \left\langle v_{\mathrm{n}}(T) \right\rangle N_{\mathrm{C}}(T) \exp\left(-\frac{\Delta G(T)}{k_{\mathrm{B}}T}\right) \tag{2.7}$$

The change in Gibbs free energy $\Delta G(T)$ is related to the associated changes in ionization enthalpy (ΔH) and entropy (ΔS) by the thermodynamic identity

$$\Delta G(T) = \Delta H - T\Delta S \tag{2.8}$$

So Eq. 2.7 becomes

$$e_{\mathrm{n}}(T) = \sigma_{\mathrm{n}} \left\langle v_{\mathrm{n}}(T) \right\rangle N_{\mathrm{C}}(T) \exp\left(\frac{\Delta S}{k_{\mathrm{B}}}\right) \exp\left(-\frac{\Delta H}{k_{\mathrm{B}}T}\right) \tag{2.9}$$

On the assumption, that the concentration of the deep levels N_{T} is small in relation to the concentration of the shallow acceptors N_{D}, the capacity-transient $\Delta C(t)$ of a Schottky contact is related to the local transient of occupied traps $\Delta n_{\mathrm{T}}(x,t)$ by

$$\Delta C(t) = -\frac{C_o}{N_{\mathrm{D}}} \frac{1}{w_o^2} \int_0^\infty \Delta n_{\mathrm{T}}(x,t) x \, dx \tag{2.10}$$

where x is the distance from the contact.

For point defects, emission and capture rate, R_{e} and R_{c}, are linearly dependent on the occupation ratio f of the defect level, so that $\Delta C(t)$ is exponentially dependent on time during capture and emission. The analysis of the DLTS-line variations with correlation frequency f and filling pulse duration t_{p} is then straightforward and yields the level of the defect (ionisation enthalpy and entropy), its electron or hole capture cross section, σ_{n} or σ_{p}, and its concentration N_{T} (see section 3.7).

2.3.2 Extended defects

DLTS is a well-established technique to investigate deep levels associated with point defects in semiconductors. For spatially extended defects, asymmetrically[49] or symmetrically[50] broadened DLTS lines are frequently observed together with a logarithmic capture law in a certain range of filling pulse lengths, t_p, i.e. $\Delta C_\mathrm{max} \propto \ln(t_\mathrm{p})$[51, 52, 53, 54] where ΔC_max denotes the amplitude of the DLTS line.

Recent modelling of extended defects on the basis of a density of states, $N(E)$, and a capture barrier, δE_C, associated with an extended defect, have made evident, that states and levels have significantly different characteristics. It has also been shown, that even for a distribution of levels, each of which exchanges electrons only with the conduction or valence band, the rate equations of all levels remain coupled through the common capture barrier, depending on the occupation of all levels.

The capture rate of each spectral component, $R_\mathrm{c}(E)$, is affected by the total occupation of the extended defect states, F, and by the screening charge through the Coulombic interaction. This effect is described in Figure 2.1 for an extended defect in n-type silicon by a capture barrier δE_c.

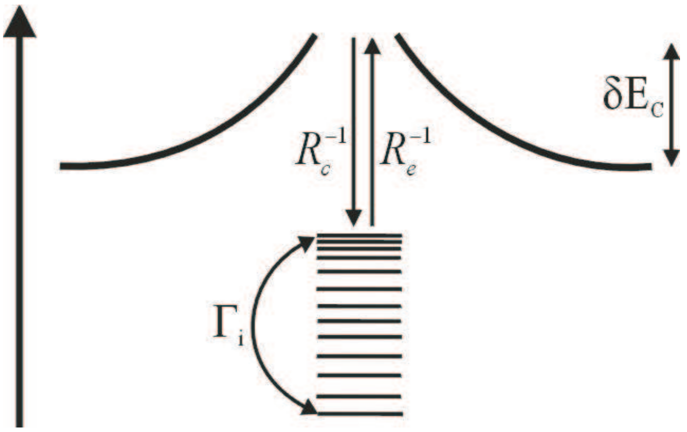

Figure 2.1: Band diagram of the electronic conditions at an extended defect. dE_c denotes the capture barrier for electrons, R_e^{-1} and R_c^{-1} inverse emission and capture rate, respectively, and Γ_i the time needed for internal equilibration of electrons in defect states.

Model calculations have shown[55], that the broadening of the spectrum goes back to a distribution of defect states $N(E) = \rho(E)N_\mathrm{T}$ in the gap of the semiconductor. $\rho(E)$ describes here the normalized density of states.

For an extended defect with an occupation degree F^N in the neutral state, the capture barrier may be expressed as,

$$\delta E_{\mathrm{c}} = \alpha(F - F^{\mathrm{N}}) \tag{2.11}$$

with the capture barrier coefficient $\alpha \geq 0$ as proportionality factor. In the case of an occupation $F > F^{\mathrm{N}}$ the defect is negatively charged, for an occupation $F < F^{\mathrm{N}}$ the interaction becomes attractive for electrons and repulsive for holes.

The rate equation of the point defect extended by the capture barrier reads without consideration of a distribution of defect conditions $N(E)$:

$$\frac{\partial f}{\partial t} = c_{\mathrm{n}} \exp\left(-\frac{\delta E_{\mathrm{c}}}{k_{\mathrm{B}}T}\right)(1 - f) - e_{\mathrm{n}} f \tag{2.12}$$

A parameter, that strongly affects the emission behaviour of extended defects, is the internal equilibration time Γ_{i}, which is the time it takes to establish electronic equilibrium at the defect. Γ_{i} reflects the origin and distribution of the extended defect deep states. When compared to the inverse carrier emission rate R_{e}^{-1} and inverse capture rate R_{c}^{-1}, it allows to distinguish between "bandlike" states ($\Gamma_{\mathrm{i}} \ll R_{\mathrm{e}}^{-1}, R_{\mathrm{c}}^{-1}$) and "localised" states ($\Gamma_{\mathrm{i}} \gg R_{\mathrm{e}}^{-1}, R_{\mathrm{c}}^{-1}$), i.e. interact in such a way that individual defect states almost exclusively exchange charge carriers with conduction band or valence band. The rate equation 2.12 has to be modified to

$$\frac{\partial f_{\mathrm{i}}}{\partial t} = c_{\mathrm{n}} n \exp\left(-\frac{\alpha\left(F - F^{\mathrm{N}}\right)}{k_{\mathrm{B}}T}\right)(1 - f_{\mathrm{i}}) - e_{\mathrm{n}}(E_{\mathrm{i}}) f_{\mathrm{i}} \tag{2.13}$$

where index i denotes the number of the localized states of the defect.

For bandlike states, the internal equilibration rate regulates the distribution of electrons in the defect states and adjusts it at any time during capture and emission to a Fermi distribution with a quasi- Fermi levels (E_{qF}). Fast internal equilibration makes it possible to describe the occupation of the energy levels with the help of the quasi-Fermi energy as,

$$f(E) = \frac{1}{1 + \exp\left(\frac{\alpha(F - F^{\mathrm{N}}) + E - E_{\mathrm{qF}}}{kT}\right)} \tag{2.14}$$

$$\frac{\partial F}{\partial t} = c_{\mathrm{n}} n \exp\left(-\frac{\alpha\left(F - F^{\mathrm{N}}\right)}{kT}\right)(1 - F) - \int \rho(E) e_{\mathrm{n}}(E) f(E) dE \tag{2.15}$$

A detailed representation of the model is provided by Hedemann[55] above.

DLTS measurements of extended defects make possible to differentiate between localized and bandlike conditions, by studying the behaviour of the spectra with a pulse length variation.

For localized states the characteristic features are:

(i) the maximum of the DLTS line remains with pulse length variations at the same temperature.

(ii) after the curves are normalized on a common maximum, the high temperature sides coincide.

(iii) over a large pulse length range the amplitude, of the DLTS-line increases logarithmically, i.e. $\Delta C_{\mathrm{max}} \sim \ln(t_{\mathrm{p}})$.

For bandlike states the characteristic features are:

(i) the position of the maximum of the DLTS lines shifts with larger pulse lengths to lower temperatures.

(ii) the high temperature flanks coincide without further normalization.

(iii) the absolute height of the maxima with different pulse lengths hardly rises with larger pulse lengths.

Chapter 3

Experimental work

The experiments performed in this work can be broadly separated into three stages. First, iron was deposited thermally on the sample surface. Secondly, iron was in-diffused from the surface source into the wafer by using a vertical furnace[56]. Iron concentration in the doped samples was set using known iron solubility relationship[14] above. Following the in-diffusion, the iron rich surface region was mechanically and chemically removed. The samples were annealed at different temperatures and times. Finally, Al/Si Schottky barriers were formed on the polished front surface by thermally evaporating aluminium.

The following sections describe the experimental details of the sample preparation, iron deposition, sample heat treatments, sample electrical characterisation and analysis via DLTS.

3.1 Sample preparation

The experiments were performed using p-type samples grown by the Float zone technique (Company Wacker Chemitronic) with 625 μm thickness and 1×10^{15} cm^{-3} boron concentration. Specimens were of a rectangular geometry, as described in Figure 3.1, with long edges parallel to <100> directions.

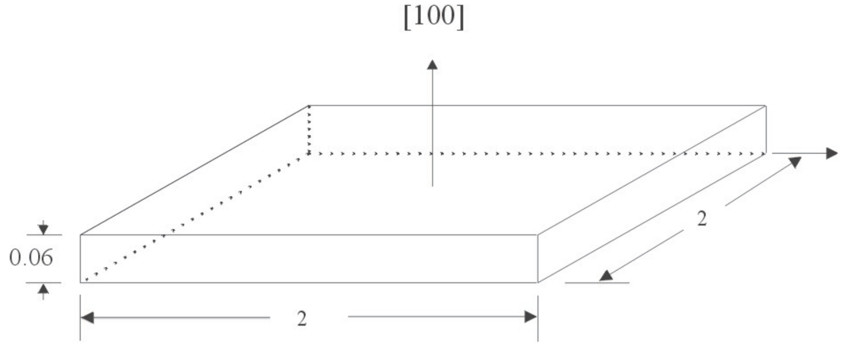

Figure 3.1: Geometry of the diffusion samples. The lengths are indicated in cm.

The chemical cleaning of the samples immediately prior to each anneal or evaporation step took place in order to remove the contaminations on the sample surfaces. The type of contaminates range from organic compounds to metallic impurities that are encountered by handling or processing. After a deionized water rinse to remove the fine particles on the wafer surface, the samples were immersed in acetone and methanol to remove the organic compounds. After that, the samples were rinsed in deionized H_2O to remove the residual of organic solvents. Ultrasonic bath was used in all cleaning steps. The atomic contaminant presents on silicon surfaces that are of the most serious concern are transition metals (TM) such as gold, iron, copper and nickel. The removal of these TM requires reactive agents, which dissolve them and form metal complexes to prevent redeposition from the solution. Therefore, the samples were immersed in the reactive agent $1HF(40\%):10HNO_3(65\%)$ for 30 to 60 seconds to remove further metallic impurities. The rest of the etching solution is eliminated by rinsing in deionized water. The native oxide was removed immediately prior to annealing by using $1HF:10H_2O$ for 20s. Thereafter the sample was fixed into a teflon mask and put quickly into the high vacuum-evaporating chamber.

The teflon tweezers and deposited teflon mask were cleaned before using in a deionized water and acetone to remove organic contamination. Finally, they were immersed in $1HF:10HNO_3$ to remove any heavy metals.

3.2 High vacuum equipment

The evaporation of iron on the silicon surface took place in a High Vacuum (HV) equipment. The tungsten boat (W) and the iron wire (1 mm diameter and 99.9985% purity from Johnson Matthey GmbH, Germany) were cleaned by immersion in boiling aceton, boiling methanol and etched afterwards in hydrochloric acid (37%) for 15 minute. The pressure in the HV chamber was below 6×10^{-7}mbar and 2×10^{-6}mbar before and during deposition, respectively. The thickness of the deposited iron layer on the sample surface was recorded by using the quartz oscillator of a layer thickness measuring instrument (Balzers). Immediately after deposition, the sample was put into the vertical furnace.

3.3 Solubility of iron in silicon

In order to produce iron in silicon with different concentrations, the iron in-diffusion temperatures and times were varied between 950 to 1200°C and 20 to 60 minutes, respectively, according to the following relation[14]

$$c_{\mathrm{Fe}} = 5 \times 10^{22} \exp\left(\frac{S_{\mathrm{M}}}{k_{\mathrm{B}}}\right) \exp\left(-\frac{Q_{\mathrm{M}}}{k_{\mathrm{B}}T}\right) \quad , \quad \mathrm{cm}^{-3} \tag{3.1}$$

where c_{Fe} is the solubility, S_{M} is the solution entropy and Q_{M} is the solution enthalpy. The entropy and enthalpy are 8.2 k_{B} and 2.94 eV, respectively, in the temperature range 900-1206°C. Table 3.1 describes the experimental conditions of the iron in-diffusion.

3.4 The vertical furnace

The used vertical furnace enabled us to obtain well defined cooling procedures (as opposed to the horizontal furnace) because the samples fall free and quickly into the quenching bath. The temperature was adjusted by using the temperature regulator 808P from Eurotherm international.

T_{D} (°C)	D (10^{-6} cm^2/s)	c_{Fe} (10^{15} cm^{-3})	t (min)
0950	2.04	0.13	60
1050	3.33	1.13	45
1100	4.13	2.88	35
1150	5.06	6.90	25
1200	6.11	15.6	20

Table 3.1: The experimental conditions of the iron diffusion annealing, T_{D} designates the diffusion temperature, D the diffusion coefficient[14], c_{Fe} the solubility of iron and t the annealing time. D has been measured between 30°C and 1250°C.

To prevent any contamination, the sample holder in the furnace (shovel) was made from quartz glass (Suprasil). The sample is put on the shovel and leaned forward directly before a small hole in the tube. The other tube serves as an admission of the Pt-PtRh-thermocuple, which permits to measure the temperature.

Inert gas (argon 99.996%) was used during the heat treatments to avoid thermal oxidation. The iron was in-diffused for long time to ensure a uniform distribution throughout the thickness of the material and to establish the Fe equilibrium solubility. The sample is kicked by a short argon impact of approximately 0.4 bar by the gas gun through the hole in the pipe into the quenching medium. The fall time is approximately 0.4 second. Annealing was terminated by quenching into ethylene glycol (estimated quenching rate ∼1000 K/s).

3.5 Preparation of diode contact

The DLTS technique requires high quality diode contacts with low leakage currents and clean interfaces. The samples were thinned from both sides to a final thickness of ≈ 400 μm using boron carbide to remove the iron silicide, which was formed during the in-diffusion. The diode was prepared as follows: first, any active layer (i.e. diode contact) on the processed sample surface was mechanically polished until a mirroring surface was achieved. The polished surface was rigorously cleaned. The cleaning procedure was similar to that used for annealing treatment for in-diffusion but without HF dip to leave the oxide layer, which is used with evaporated Al to perform the diode.

After chemical cleaning, the sample was installed immediately into HV evaporating chamber. With a pressure of $p \sim 2-5\times10^{-5}$mbar, Al was deposited from a W filament on the sample surface as diode contact. The metal pattern was defined by holes in the deposited mask. The diameter of these holes is 1 mm. Ohmic contact were made by scratching a Ga/Al alloy on the back surface.

3.6 C-V characteristics

The measurement of capacitance as a function of voltage for a diode barrier formed on a semiconductor is a routine method for evaluating some of the defect properties. The high frequency capacitance is measured as a function of bias voltage, and the free carrier density (N_{D}) is calculated from the slope of a $1/C^2$ vs V plot using the following well-known expressions:

$$C_o = \frac{\varepsilon\varepsilon_o A}{w_o} \tag{3.2}$$

$$N_{\mathrm{D}} = \frac{-2}{e\varepsilon\varepsilon_o A^2}\left(\frac{\Delta C_o^{-2}}{\Delta U_{\mathrm{B}}}\right)^{-1} \tag{3.3}$$

where w_o is the depletion layer width for a reverse bias voltage, ε is the dielectric constant, ε_o is the permitivity of free space, A is the contact area, C_o is the capacitance for a reverse bias U_{B} and N_{D} is the density of shallow impurities at the edge of the depletion region. From the intercept of the straight line with the x-axis, the built-in voltage (U_{bi}) is calculated using equation

$$C = A\left(\frac{\varepsilon\varepsilon_o N_{\mathrm{D}}}{2}\right)^{\frac{1}{2}}\left(U-\frac{k_{\mathrm{B}}T}{e}\right)^{-\frac{1}{2}}, \text{ where } U = U_{\mathrm{B}}+U_{\mathrm{bi}} \text{ [57].}$$

The carrier concentration and the built-in voltage were calculated and are given in Table 3.2.

Sample	N_D, $[10^{15}\ \mathrm{cm}^{-3}]$	U_{bi}, [V]
Fe0950-250-15	1.11	2.20
Fe1050-250-15	0.70	2.00
Fe1100-250-15	0.86	2.00
Fe1100-200-30	0.91	2.30
Fe1150-200-15	0.40	1.80
Fe1150-200-30	0.89	2.30
Fe1200-200-15	1.12	1.88
Fe1200-200-30	0.87	1.93
Fe1200-200-120	0.68	2.30
Fe1200-250-15	0.78	2.14
Fe1200-250-30	1.19	2.30
Fe1200-250-120	0.98	2.27
Fe1200-550-15	1.08	2.50

Table 3.2: The carrier concentrations (N_{D}) and built-in voltage (U_{bi}) were calculated from equation 3.3.

3.7 Trap concentration

One can determine the concentration of the deep levels from the height of the maximum DLTS signal, which corresponds to the change of the diode capacity $2\Delta C/C_o$ immediately after the end of the pulse. If the deep levels are homogeneously distributed, applies:

$$n_{\mathrm{T}} = \frac{2\Delta C(t_{\mathrm{p}} = \infty)}{C_o} N_{\mathrm{D}} \frac{w_o^2}{\lambda_{\mathrm{e}}^2 - \lambda_{\mathrm{c}}^2} \tag{3.4}$$

$\lambda_{\mathrm{e,c}}$ the intersection of the defect level with the Fermi level during emission (λ_{e}) or capture process (λ_{c}), U_{bi} is the built-in voltage, U_{B} the reverse voltage and w_o the width of the space-charge region. Equation 3.4 requires that after the pulse of the duration t_{p} all deep levels are occupied (saturation). For $U_{\mathrm{B}} = U_{\mathrm{P}}$, $\lambda_{\mathrm{c}} \approx 0$ can be set and one maintains a simple formula indicated by Mircea and Mitonneau[58]

$$N_{\mathrm{T}} = \frac{2\Delta C_{\max}(t_{\mathrm{p}} = \infty)}{C_o} N_{\mathrm{D}} \frac{1}{\left(1 - \sqrt{\frac{E_{\mathrm{T}} - E_{\mathrm{F}}}{q(U_{\mathrm{bi}} + U_{\mathrm{B}})}}\right)^2} \tag{3.5}$$

From equation 3.5, one can calculate the trap concentration.

3.8 Correlation function

In this work DLTS was based on the direct recording and analysis of capacitance transients. This method is similar to correlation techniques and is based on scanning the sample temperature (and thereby changing the deep level transient time constant) under a set of time constant of the measuring apparatus.

Thus the acquisition of the capacitance data is separated from the signal processing which is done by the computer afterwards. The entire measurement is controlled by computer and the experimental data are digitally stored for the analysis.

The correlation of the signal takes place computationally (software) via integration of the product of transient ($A_o \cdot \exp(-e_{\mathrm{p}}t)$, where A_o is the amplitude) and a correlation function during one period. In our example the correlation function is $\sin\left(\frac{2\pi}{T_o}t\right)$, which simulates Lock-in amplifier in with the phase shift t_φ of $\frac{t_{\mathrm{g}}}{2}$.

$$S(e_{\mathrm{p}}) = \frac{1}{T_o} \int_{t_\varphi}^{T_o + t_\varphi} A_o \exp\left(-e_{\mathrm{p}}t\right) \sin\left(\frac{2\pi}{T_o}t\right) \, dt \tag{3.6}$$

where , $t_{\mathrm{g}} = t_{\mathrm{p}} + t_{\mathrm{a}}$ and t_{a} is the delay time (in this work =100 μs). The time period T_o determines the reference time constant, and is the reciprocal of the frequency, f, of the Lock-in amplifier.

Figure 3.2 illustrates the operation of a system:

(i) shows the sample bias pulses;

(ii) the transient signal and;

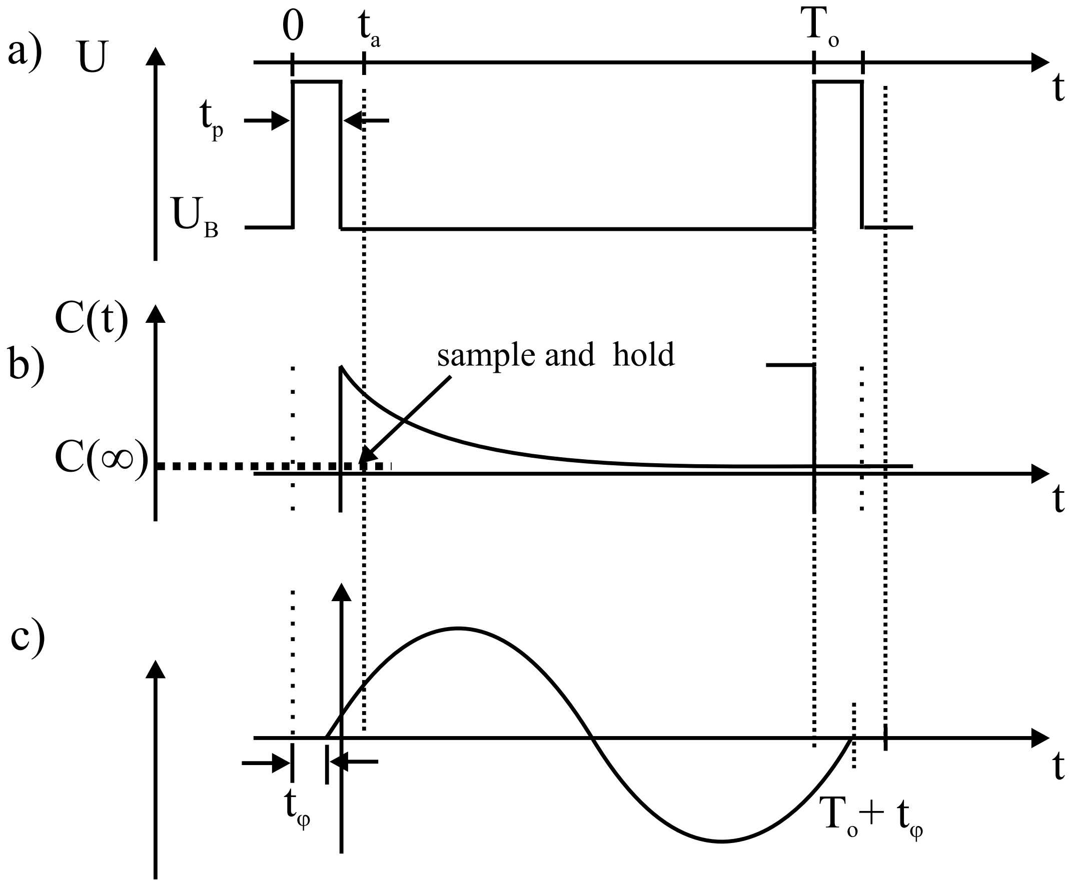

Figure 3.2: Correlation of the capacitance-transient: (A) reverse voltage U_B applied by a periodic pulse voltage, (b) capacity-transiently, (C) sinusoidal correlations function with a phase shift t_f of $t_\mathrm{g}/2$.

(iii) the correlation function.

The signal in the interval filling pulse (t_p) and instruments recovery delay time (t_a), the latter being when the capacitance meter is overloaded because C is very large at low bias, does not contain useful information. In addition, the both completely distort the operation of the system as a rate window. Therefore, sample and hold technique was used to eliminate that time interval and hold the input signal at its value at the end of the transient decay (Figure 3.2).

At the temperature of the maximum the ratio of emission rate e_p and pulse repetition frequency f is given by a constant value dependent on the correlation function $\alpha = f/e_\mathrm{p} = f\tau$, where $\tau = 1/e_\mathrm{p}$. The maximum of this-line shape function occurs for $\tau_{\text{max}} = 0.424T_o$. This is the Lock-in DLTS rate-window relationship for capacitance transients.

The spectrum of a point defect has the typical behaviour shown in figure 3.3 for frequency variation ($f_1 < f_2 < f_3$).

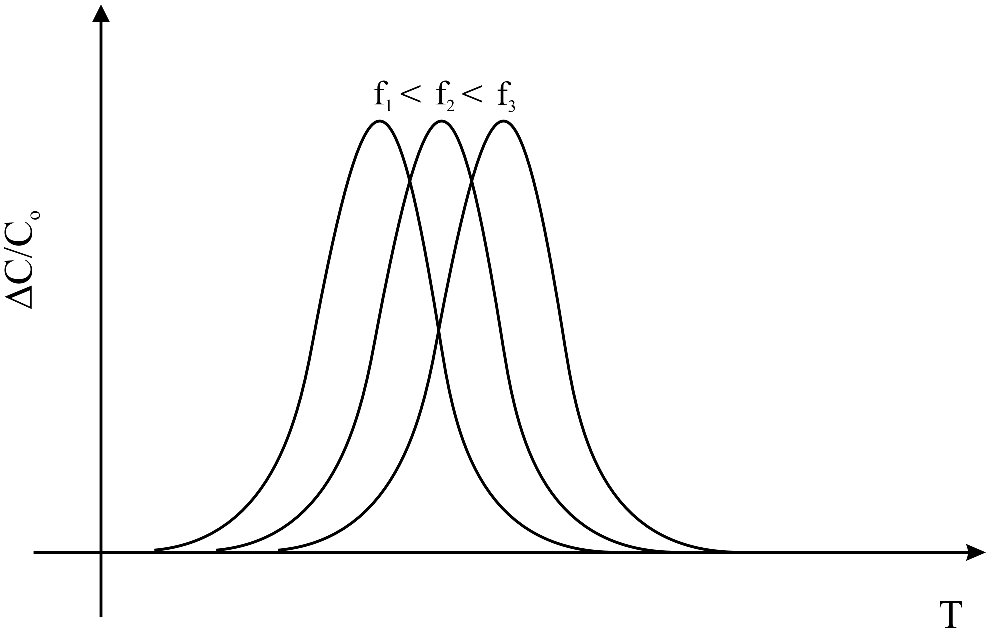

Figure 3.3: Typical behaviour of a point defect spectrum for three different pulse repetition frequencies.

3.9 The measurement condition

DLTS has the drawback that the line shape becomes distorted if the trap concentration is not negligible in comparison to the shallow dopant density. Therefore, the equation 3.5 is valid only when the free carrier density is much larger than the density of deep levels.

The samples were doped with iron by in-diffusion at different temperatures for different times (see table 3.1) and subsequently were annealed at different temperatures for different times. The samples were named and abbreviated according to those parameters as follows;

(i) diffusion temperature, abbreviated (FeT_D, e.g. Fe950-00-00),

(ii) annealing temperature, abbreviated (FeT_D-T_A, e.g. Fe950-200-00),

(iii) annealing time, abbreviated (FeT_D-T_A-t_A, e.g. Fe950-200-30),

(iv) and the reference sample (without iron), abbreviated (–950-250-30).

Chapter 4

Results

It is known, that iron can exist in B-doped silicon in the following states:

(i) Single interstitial iron ($\mathrm{Fe_i}$) atoms: At room temperature they are thermodynamically not stable[18, 59]. However, if a specimen, doped by Fe to concentration of about (or below) its solubility at high temperature, is quenched to room temperature, a major fraction of iron remains in a form of isolated Fe atoms in interstitial sites ($\mathrm{Fe_i}$).

(ii) (FeB)-pairs: After quenching to room temperature, $\mathrm{Fe_i}$ slowly (within days) reacts with boron to form (FeB)-pairs. In equilibrium, the ratio $c_{\mathrm{FeB}}/c_{\mathrm{Fe_i}}$ decreases exponentially with increasing temperatures and becomes smaller than 3% at 200°C.

(iii) Iron precipitates: Since the solubility of Fe is very low at room temperature, Fe should tends to form a precipitates, that can be dissolved only at high temperature[15, 60], when the solubility becomes higher than Fe concentration. So, the interstitial iron can be converted to iron precipitates by a proper annealing[15, 18].

It has been reported by several researchers[15, 18, 61], that iron in boron-doped p-type silicon forms two donor levels at $(E_{\mathrm{V}} + 0.4)$ eV and $(E_{\mathrm{V}} + 0.1)$ eV, and that the former is assigned to a level due to interstitial iron and the latter is assigned to the iron-boron complex.

In our experiments the boron concentration was at $N_{\mathrm{D}} = 1 \times 10^{15}$ cm^{-3}, while the concentration of N_{T}, was varied by varying the temperature (T_{D}) at which sample was saturated by iron by diffusion from $\mathrm{FeSi_2}$ layer on the surface into the wafer (see Table 3.1). The condition $N_{\mathrm{T}} \ll N_{\mathrm{D}}$, necessary to be able to measure the initial distribution of $\mathrm{Fe_i}$ by DLTS, is satisfied only for $T_{\mathrm{D}} = 950°\mathrm{C}$. In this condition we were able to check whether our sample preparation conditions are clean enough and the iron is the only transient metal impurity introduced into our samples during our sample preparation steps. To make this check we:

(i) Compare our DLTS data with the $\mathrm{Fe_i}$ and FeB-pairs deep level positions and capture cross sections, published in a literature.

(ii) Measured the total iron concentration by DLTS using equation 3.5 when all iron is in the form of $\mathrm{Fe_i}$ and compare it with predicted iron solubility.

4.1 DLTS of interstitial iron

The DLTS spectrum for the sample Fe950-00-00, which was saturated by at 950°C and stored for several days at room temperature after quenching, is given in Figure 4.1. This figure shows that there is only one DLTS-line at 55 K and no other lines in the temperature range from 50 to 300 K.

The energy level and the capture cross section are important parameters for identifying nature of deep level. These parameters can be calculated using Eq. 2.9 from the thermal emission rate, measured as a function of temperature using different correlation rate windows.

For the DLTS-line shown in Figure 4.1, the logarithm of the thermal emission rate of holes from the defect to valence band divided by the square of the temperature T is plotted versus the inverse temperature is in the inset of Figure 4.1. This plot is

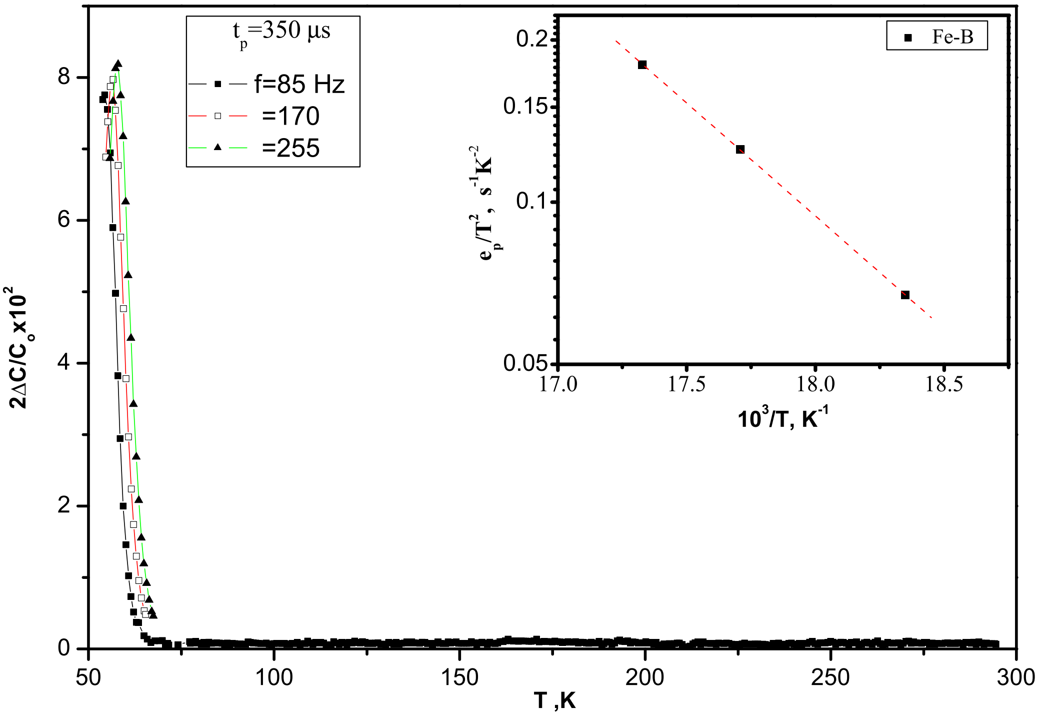

Figure 4.1: Majority-carrier (hole) DLTS spectrum of iron-doped FZ p-type which was in-diffused at 950°C for 60 minutes and stored at room temperature a several dayes. Measuring condition of DLTS: the filling pulse duration $t_{\mathrm{p}} = 350$ μs and reverse bias $U_{\mathrm{B}} = 3$ V and filling pulse bias $U_{\mathrm{p}} = 2.8$ V. **Inset Figure:** Thermal emission rates (T^2 corrected) as a function of inverse temperature for FeB line observed in the sample which iron was in-diffused at 950°C.

called the emission characteristic of a point defect and, by a comparison with literature data, may be used to identify the defect. The energy level E_{T} and the capture cross section σ_{p} of the defect can be determined from the slope and the intercept of the straight line by the least-mean-square method on the assumption that σ_{p} is temperature independent.

From the Arrhenius plot, shown in the insert in Figure 4.1 we have found both parameters for the DLTS line shown in Figure 4.1: the enthalpy (activation energy) is $E_{\mathrm{T}} = \Delta H = 0.097$ eV and the hole capture cross section $\sigma_{\mathrm{p}} = 1.69 \times 10^{-14}$ cm^2. These are very close to the emission rate characteristic and capture cross section of the FeB complex: $E_{\mathrm{T}} = 0.09$eV and $\sigma_{\mathrm{p}} = 2 \times 10^{-14}$ cm^2, respectively, reported in[16] and [18].

Therefore, the observed DLTS line (see Figure 4.1) can be attributed to the donor level of FeB pairs. This is what we could expect. Indeed, the ratio of pair concentration to concentration of $\mathrm{Fe_i}$, $(\mathrm{FeB})/(\mathrm{Fe_i})$ is proportional to $\exp(U_{\mathrm{FeB}}/kT)$, where U_{FeB} is pair binding energy of about 0.65eV. So, the equilibrium concentration of pairs at room temperature should be much higher than of isolated $\mathrm{Fe_i}$. At the same time, the kinetic of pair formation is determined by the migration energy of $\mathrm{Fe_i^+}$, which is also about 0.65eV, so that association and dissociation of pairs occurs already at room temperature and storing the sample several days at room temperature is enough to establish the equilibrium between $\mathrm{Fe_i}$ and FeB.

The concentration of the traps N_{T}, related to FeB can be evaluated from the line amplitude of the spectrum shown in Figure 4.1 using Eq. 3.5. For the concentration of $(\mathrm{Fe_iB})$ pairs we obtained 1.3×10^{14} cm^{-3} that is in excellent agreement with the solubility of iron equal to 1.3×10^{14} cm^{-3} at the diffusion temperature 950°C.

Formation and dissociation of iron-boron pairs

One more critical check that we really have an iron in our sample and no more transient metal is to observe the dissociation of $\mathrm{Fe_iB_s}$ pairs and appearance of the DLTS signal from $\mathrm{Fe_i}$. This was observed for the first time by Kimerling and Benton[62]. So, we have measured the DLTS in the same sample, as in Figure 4.1 after its annealing at 200°C for 30 minutes to destroy the FeB-pairs. The result is shown in Figure 4.2. It gives the evidence for the dissociation of iron-boron pairs due to the thermal annealing.

As one can see in Figure 4.2, the amplitude of DLTS corresponding to FeB pairs has strongly decreased after annealing and, at the same time a second DLTS line has appeared around 255 K that is supposed to correspond to $\mathrm{Fe_i}$.

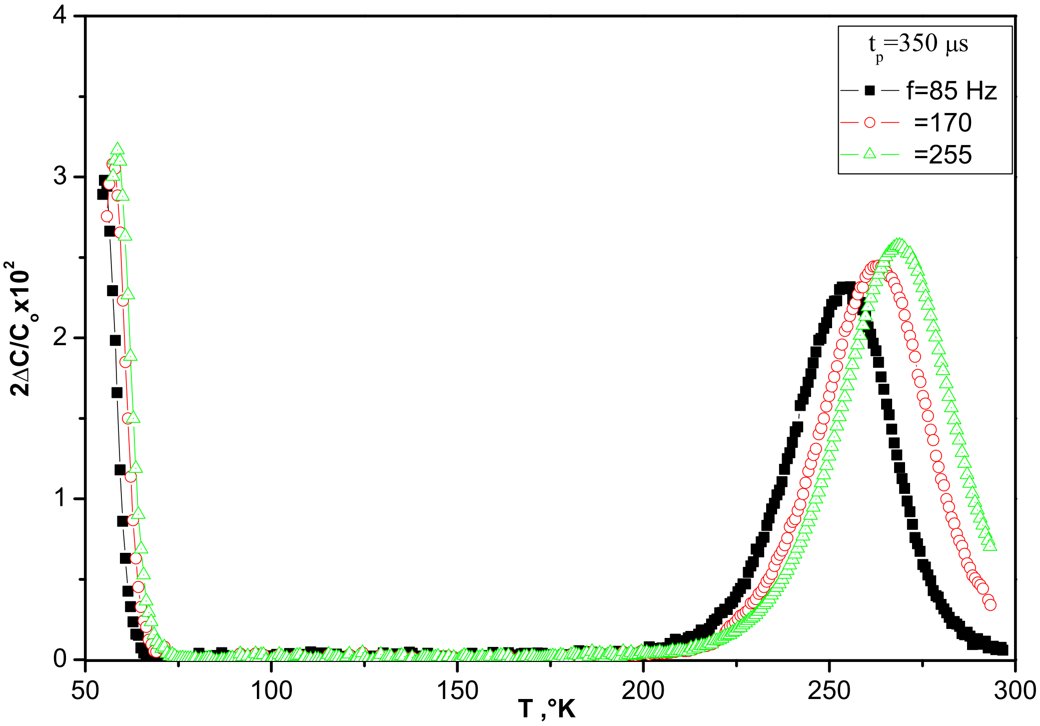

Figure 4.2: Majority-carrier (holes) DLTS spectrum of iron-doped FZ p-type which iron was in-diffused at 950°C for 60 minutes showing the dissociation of FeB to $\mathrm{Fe_i}$ after annealing at 200°C for 30 minutes. Measurement conditions of DLTS: the filling pulse duration $t_\mathrm{p} = 350\ \mu$s, reverse bias $U_\mathrm{B} = 3$ V and filling bias $U_\mathrm{p} = 2.8$ V.

The sum of the amplitudes of the two lines is approximately equal to the amplitude of the FeB line in Figure 4.1, as it should be, since some of the FeB pairs are dissociated into $\mathrm{Fe_i}$ and substitutional boron $\mathrm{B_s}$.

The emission characteristic measured for the second line is in a good agreement with those of the $\mathrm{Fe_i}$-donor level, known from a literature (see Figure 4.3). Wünstel et al. and Brotherton et al. have identified this high-temperature line as the $\mathrm{Fe_i}$ with the thermal activation energy of 0.42 eV. The energy level obtained from of our measurements is very close to the results from Brotherton et al.[16].

Therefore, the observed ionization enthalpy of $\Delta H = 0.414$ eV is attributed to

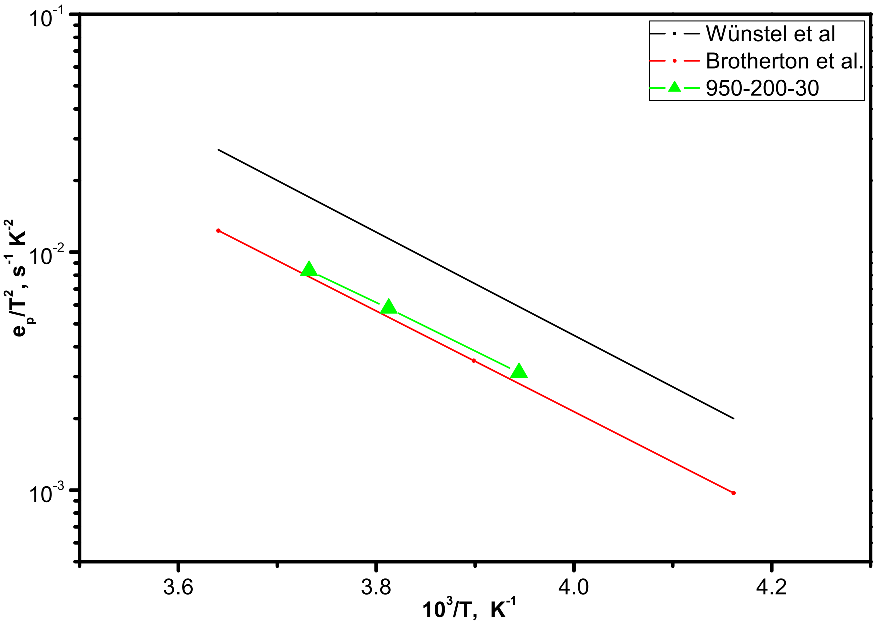

Figure 4.3: Thermal emission rates (T^2 corrected) as a function of inverse temperature for DLTS peaks observed in the sample which iron was in-diffused at 950°C. Filling pulse height $U_\mathrm{p} = 3$ V; filling pulse width $t_\mathrm{p} = 100$ μs; reverse bias $U_\mathrm{B} = 3$ V. Also included are the data from Wünstel et al.[18] and Brotherton et al.[16].

the donor level of $\mathrm{Fe_i}$. It is known that $\mathrm{Fe_i}$ has a capture barrier, i.e. $\sigma_\mathrm{p} = \sigma^* \exp\left(-\Delta H_\mathrm{cap}/k_\mathrm{B}T\right)$, so that the measured enthalpy, is $\Delta H = \Delta H_\mathrm{ion} + \Delta H_\mathrm{cap}$, where $\Delta H_\mathrm{cap} = 0.015$ eV[63].

The hole capture cross sections for FeB and $\mathrm{Fe_i}$ were calculated from the prefactors of the Arrhenius plot as 1.69×10^{-14} and 1.28×10^{-16} cm^2. These results agree with previous data associated with iron-boron pairs and interstitial iron[16, 18].

The concentrations of iron-boron pairs and interstitial iron are 6.4×10^{13} and 5.2×10^{13} cm^{-3}, respectively. The sum of the two concentrations is in fair agreement with the solubility[14] of iron in silicon at 950°C.

Figures 4.1 and 4.2 show, that no deep levels were detected except those of the iron-boron pairs and interstitial iron defects.

4.2 DLTS of iron clusters

To investigate the precipitation of iron and the influence of precipitation on electronic properties of silicon, two experimental strategies have been considered:

(i) to measure the total concentration of the dissolved iron by using DLTS. The sum of the amplitudes of DLTS lines, corresponding to the interstitial iron donor level and to the iron-boron pairs gives the concentration of dissolved iron. Any decrease of the dissolved iron concentration is assumed to be due to formation of iron precipitates. For a reliable DLTS measurements of the shallow (Fe_iB)-donor our 1MHz bridge has to be used,

(ii) to detect some new DLTS lines that can be possibly associated to the iron precipitates. Then our attention will be focused on the shape and behaviour of the DLTS line with varying filling pulse widths and frequencies. In this case a DLTS apparatus operating at our 21 MHz is preferred to cover a large filling pulse range.

The first way is appropriate to study the decay of iron supersaturation. The second which has been chosen in this work, should give an insight into the electronic structure of the iron precipitates, which develop during that decay.

4.2.1 New DLTS-line ”interstitial iron-clusters”

Figure 4.4 presents a set of DLTS spectra measured for Fe-contaminated p-type silicon after annealing at different temperatures 200 and 250°C for different times 30 and 15, respectively. A control sample (–950-250-30) was prepared at the same time under identical conditions, except for the Fe-doping (curve A).

One can see in Figure 4.4, that after annealing at 200°C for 30 minutes (see curve B), the well known FeB line and the line of interstitial iron can be observed and the total concentration of iron is about the same as in quenched sample. So, we do not see any traces of iron precipitation. However, after annealing at 250°C for 15

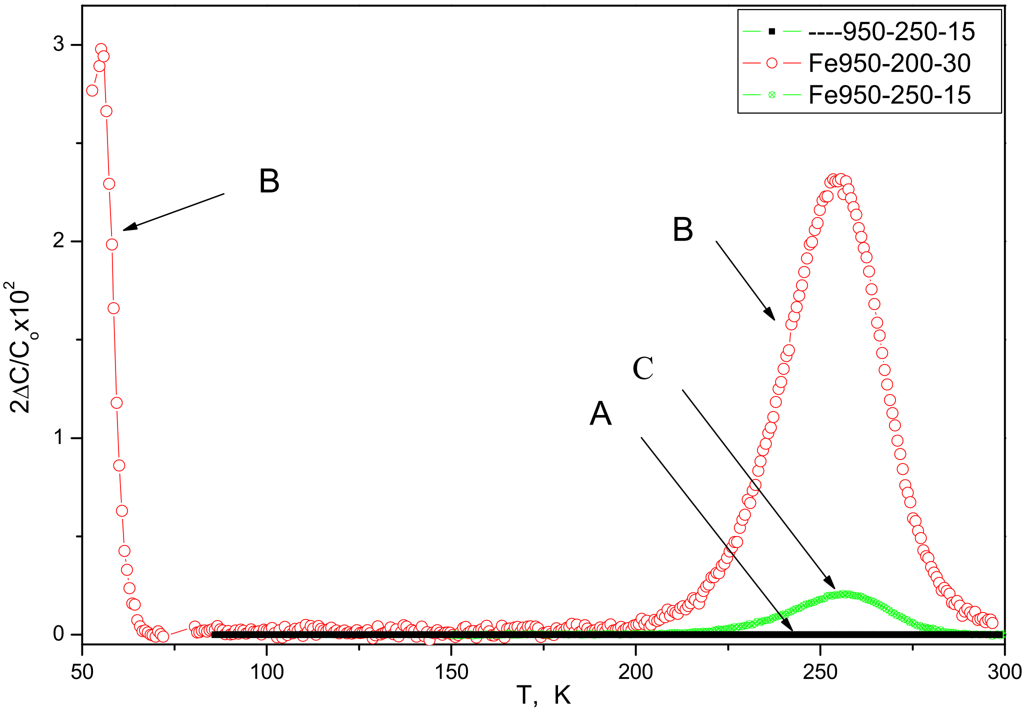

Figure 4.4: DLTS spectra for samples -950-250-15 (Line A), Fe950-200-30 (Line B) and Fe950-250-15 (Line C). The measurement conditions for sample Fe950-200-30 are filling pulse duration $t_\mathrm{p} = 350\ \mu$s, reverse bias $U_\mathrm{B} = 3$ V, filling pulse amplitude $U_\mathrm{p} = 2.8$ V and repetition frequency $f = 85$ Hz. For sample Fe950-250-15 are filling pulse duration $t_\mathrm{p} = 100\ \mu$s, $U_\mathrm{B} = 3$ V, $U_\mathrm{p} = 3$ V and $f = 68$ Hz.

minutes, concentration of dissolved iron has decreased drastically (see curve (C)). The DLTS line in spectrum (C) at $T = 256$ K looks very similar to one of $\mathrm{Fe_i}$, but its properties are quite different from the DLTS line of $\mathrm{Fe_i}$, so it is some new line.

One of the differences between properties of this new DLTS line from the usually observed for interstitial iron is its high stability on storage at room temperature. The new line is stable, so that the defects related to this line do not react with boron at room temperature. Figure 4.5 demonstrates this: it shows the new DLTS line, measured immediately after annealing at 250 °C (1^st measurement) and after storing the sample at room temperature for one month, (2^nd measurement). One can see that no significant decrease of the line amplitude happened. This gives the

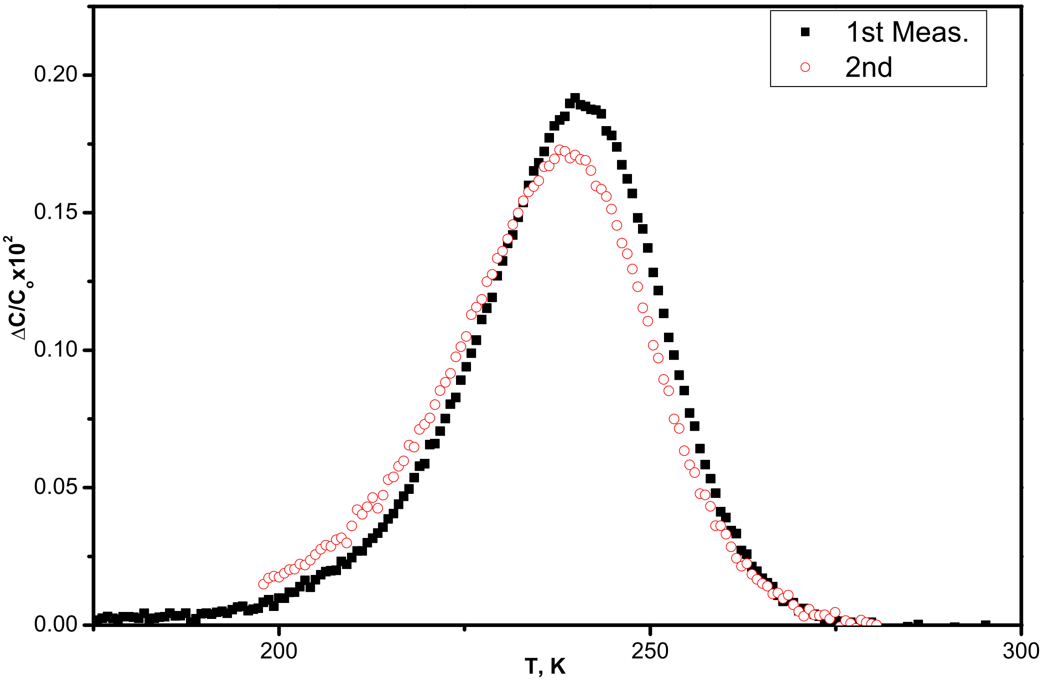

Figure 4.5: The effect of storage time in the sample Fe950-250-15 on the stability of the amplitude. The spectra were taken with the same measurement conditions.

idea that the defects responsible for the new line are not isolated interstitial iron atoms.

We will call this new line as ”interstitial iron-clusters line” for reasons we will show below.

4.2.2 The characterization of DLTS of interstitial iron-cluster line

The goal of this section is the study of the main features regarding to the new DLTS line, appeared after annealing at 250°C, for 15 minutes. Below we present some experimental evidences that this new DLTS line can be associated with the interstitial iron-clusters defect and discuss its main characteristics, such as energy level, capture cross section, capture kinetic, and its line shape.

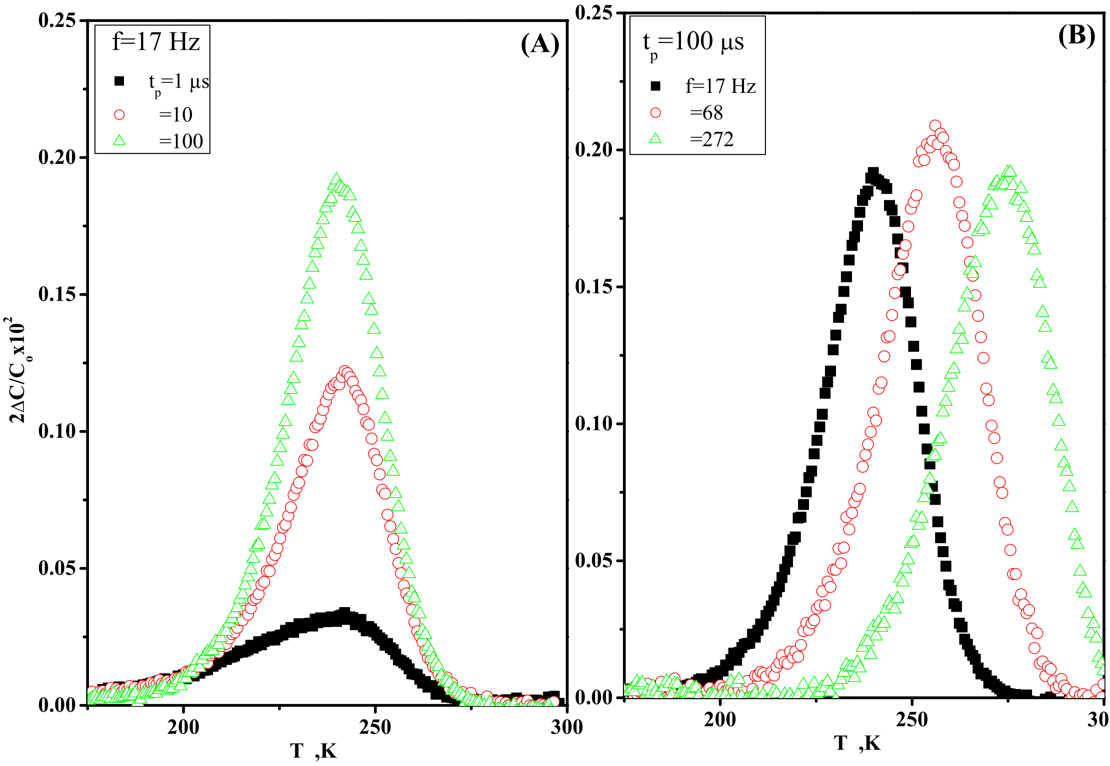

Figure 4.6: DLTS spectra after iron was in-diffused at T_D = 950°C for 60 minutes and annealed at T_A = 250°C for 15 minutes. The measurement conditions are (A) Filling pulse duration of 1, 10 and 100 μs at frequency f = 17 Hz. (B) Repetition frequency of 17, 68 and 272 Hz at filling pulse duration t_p = 100 μs.

The most powerful way to distinguish extended defects from point defects and obtain some other important parameters by DLTS is to measure the variation of DLTS spectra with varying filling pulse widths and repetition frequencies and to analyze these data in terms of existing theoretical models which allows also to differentiate between the localized and bandlike states at extended defects (see section 2.3)[47]. Note that the correlation frequency is equal to the measurement frequency.

Figure 4.6 shows typical DLTS spectra after in-diffusion of iron at 950°C and annealing at 250°C for 15 minutes. One can immediately see in Figure 4.6-A that the DLTS line shows behaviour strongly different from point defects: the amplitude of line increases with increasing filling pulse duration proportionally to log (t_p). Figure 4.6-B shows DLTS spectra measured at different correlation frequencies.

Significant features of the spectra that evolve for different pulse durations and frequencies are:

(i) all the spectra are in the form of a single line, indicative of a narrowly distributed group of energy levels,

(ii) the amplitude of the DLTS line increases logarithmically with increase of the filling pulse duration $t_{\rm p}$ and

(iii) the peak position temperature of the DLTS line is independent of filling pulse duration.

According to the two criteria of the localized state at extended defect[64], variation of line amplitude with filling pulse width should obeys a logarithmic capture law and high-temperature sides should coincide after normalization. Our DLTS line satisfies all these criteria: One can see from Figure 4.7-A, that our DLTS spectra at the high temperature sides coincide, while at the low-temperature sides small deviations appear except with $t_{\rm p} = 1$ μs line, which deviates largely.

The presence of small (below 10^{12} cm^{-3}) of some other defects could be the origin of these deviations. Figure 4.7-B illustrates, that the line amplitude indeed increases logarithmically with the filling pulse duration. For $t_{\rm p} \geq 10$ μs the line appears not broadened.

So, we can conclude, that the DLTS line that appears after annealing of Fe-doped samples 15 min at 250°C corresponds to some extended defects with localized states and very narrow distribution of energy levels in energy. At the same time, the DLTS line positions measured at different frequencies are very close to those of isolated $\rm Fe_i$ atoms. It means that the electronic energy levels of Fei are not strongly modified when iron is collected to these extended defects.

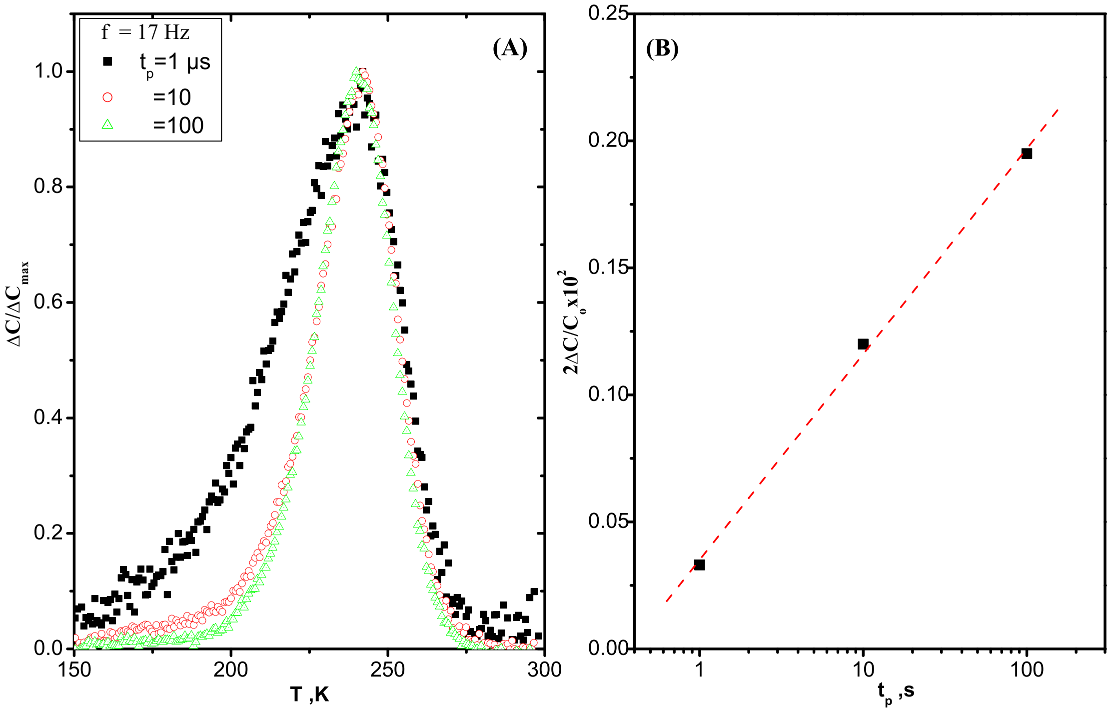

Figure 4.7: (A) Filling pulse width evaluation of the DLTS-line associated with sample Fe950-250-15. For better comparison the different spectra are normalized. The measurement conditions are (A) filling pulse duration value of respective DLTS signal; 1, 10 and 100 μs, pulse height $U_\mathrm{p} = 3$ V, reverse bias $U_\mathrm{B} = 3$ V and frequency 17 Hz. (B) The DLTS line amplitude of iron-clusters deep level as a function of filling pulse duration.

Possible nature of the observed extended defects

A structure model for the new extended defect we have observed has to combine only slight modification of electronic energy levels of $\mathrm{Fe_i}$ in silicon with a significant barrier for hole capture, coming from the Coulomb interaction of holes captured by defect. The simplest model fitting these requirements is a cluster of interstitial iron with its occupied states $\mathrm{Fe_i^+}$ coupled by some long-range interaction and its energy spectrum resulting from the superposition of only slightly shifted levels of $\mathrm{Fe_i^{(o/+)}}$.

In the following we therefore name this defect "$\mathrm{Fe_i}$-clusters". At present, direct evidence, e.g. by TEM, that such clusters exist, is missing.

4.2.3 The energy levels of "Fe_i-clusters" for samples with different Fe concentrations

The DLTS spectra shown in the Figures 4.8 to 4.10 are typical for samples Fe1050-250-15, Fe1100-250-15 and Fe1150-200-15. The features of the spectra for the all samples are similar to those of "Fe_i-clusters" observed in the sample Fe950-250-15.

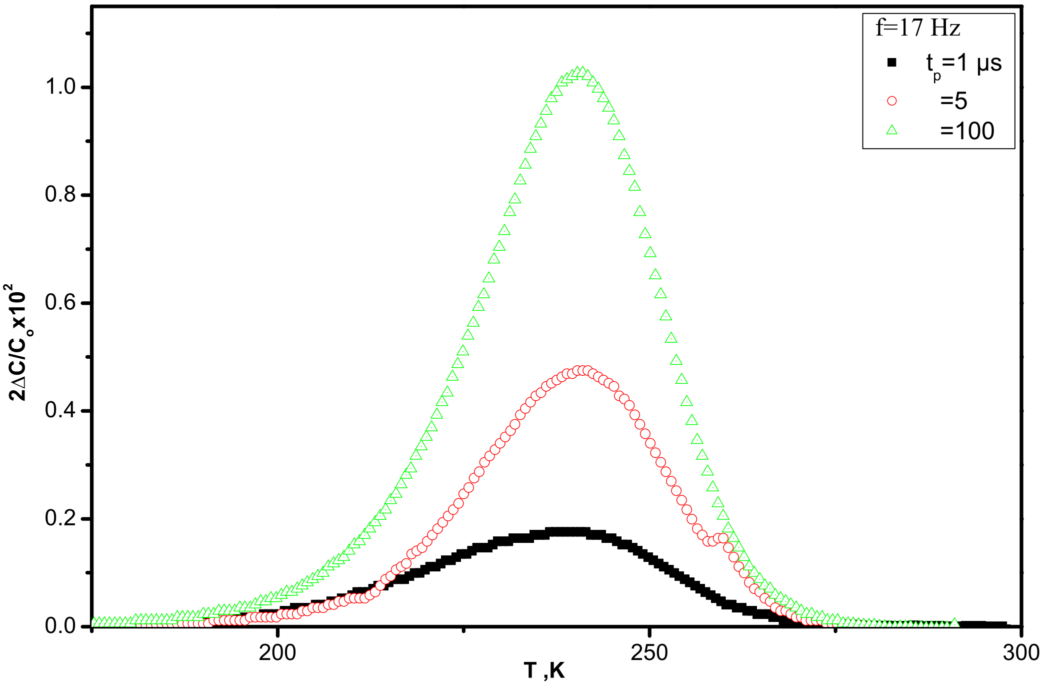

Figure 4.8: DLTS spectra for sample Fe1050-250-15. The measurement conditions are filling pulse duration of 1, 10 and 100 μs at frequency $f = 17$ Hz. The filling pulse height $U_p = 3$ V and the bias voltage $U_B = 3$ V

Figure 4.11 illustrates that the DLTS line amplitude depends on the iron concentration. One observes in the inset in Figure 4.11, that the DLTS-line amplitude increases approximately linearly with the iron concentration.

Although the DLTS lines for samples, Fe0950-250-15, Fe1050-250-15, Fe1100-250-15 and Fe1150-200-15 do not represent a point defect, we made a conventional analysis by Arrhenius plot, which yields activation enthalpies and capture cross sections as

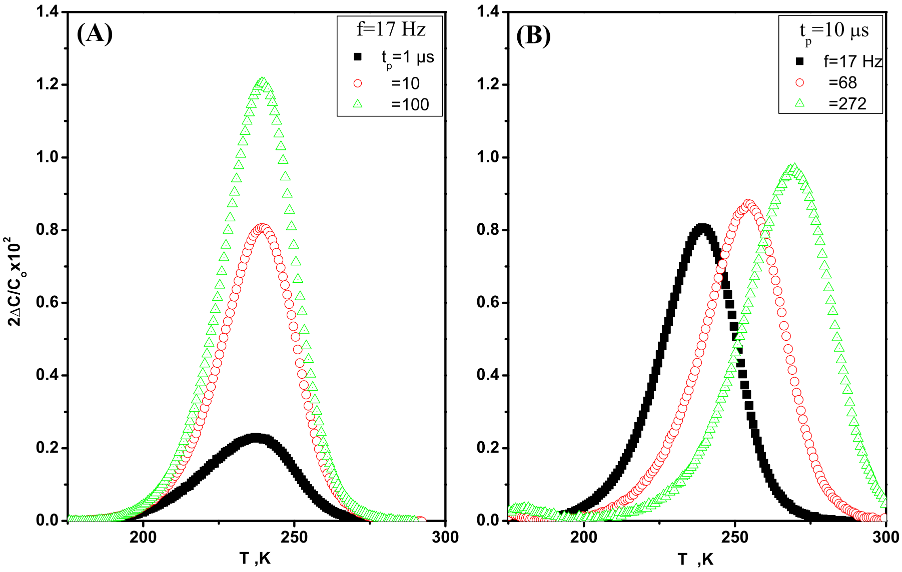

Figure 4.9: DLTS spectra for sample Fe1100-250-15. The measurement conditions are (A) Filling pulse duration of 1, 10 and 100 μs at frequency $f = 17$ Hz. (B) Repetition frequency of 17, 68 and 272 Hz at filling pulse height $t_\mathrm{p} = 10$ μs. The filling pulse duration $U_\mathrm{p} = 3$ V and the bias voltage $U_\mathrm{B} = 3$ V.

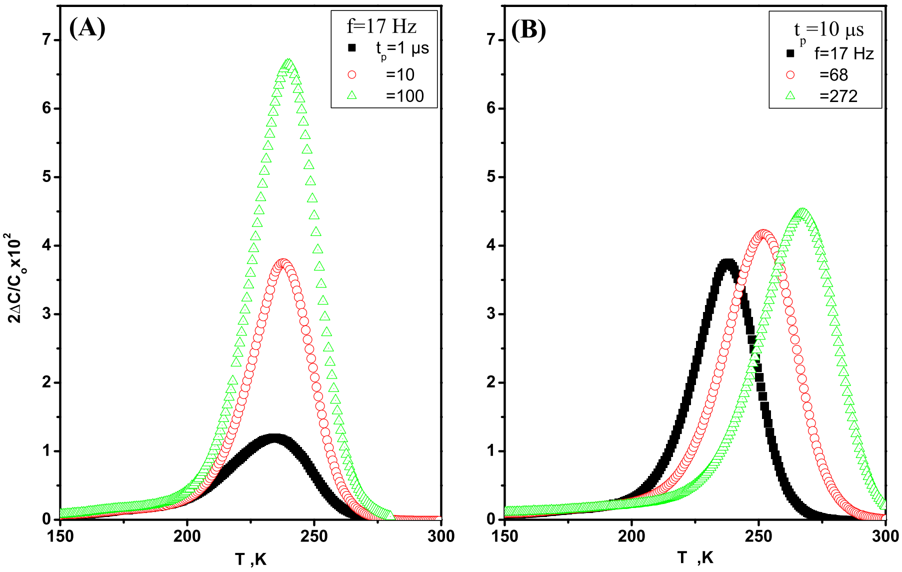

Figure 4.10: DLTS spectra for sample Fe1150-200-15. The measurement conditions are (A) Filling pulse duration of 1, 10 and 100 μs at frequency $f = 17$ Hz. (B) Repetition frequency of 17, 68 and 272 Hz at filling pulse duration $t_\mathrm{p} = 10$ μs. The filling pulse height $U_\mathrm{p} = 3$ V and the bias voltage $U_\mathrm{B} = 3$ V.

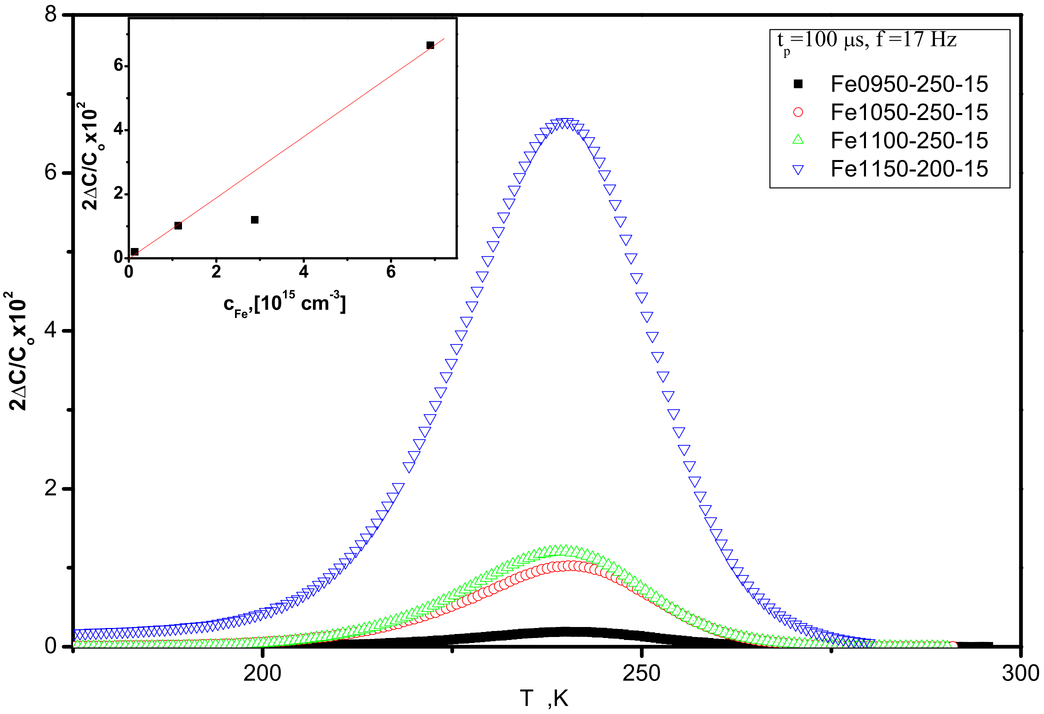

Figure 4.11: DLTS spectrum for samples Fe950-250-15, Fe1050-250-15, Fe1100-250-15 and Fe1150-200-15. The DLTS spectra were measured with filling pulse duration at 100 μs and the repetition frequency at 17 Hz. The filling pulse amplitude $U_{\rm p} = 3$ V and the bias voltage $U_{\rm B} = 3$ V.

obtained from the DLTS measurements. These values are called "apparent" since the parameters obtained for an extended defect with localized states from an Arrhenius plot have been shown to be of no physical significance, because they depend on the DLTS filling pulse duration used in the measurements[65]. However the Arrhenius plot may be seen as a condensed way of describing DLTS spectra, which is useful for comparison with published data. More than that, since the DLTS lines are not significantly broadened compared with DLTS of single energy level, for this particular case the Arrhenius plot analysis should probably give correct energy position and cross section.

Figure 4.12 presents the emission characteristics for samples Fe950-250-15, Fe1050-250-15, Fe1100-250-15 and Fe1150-200-15 and that of interstitial iron donor as reported by Brotherton et al.[16].

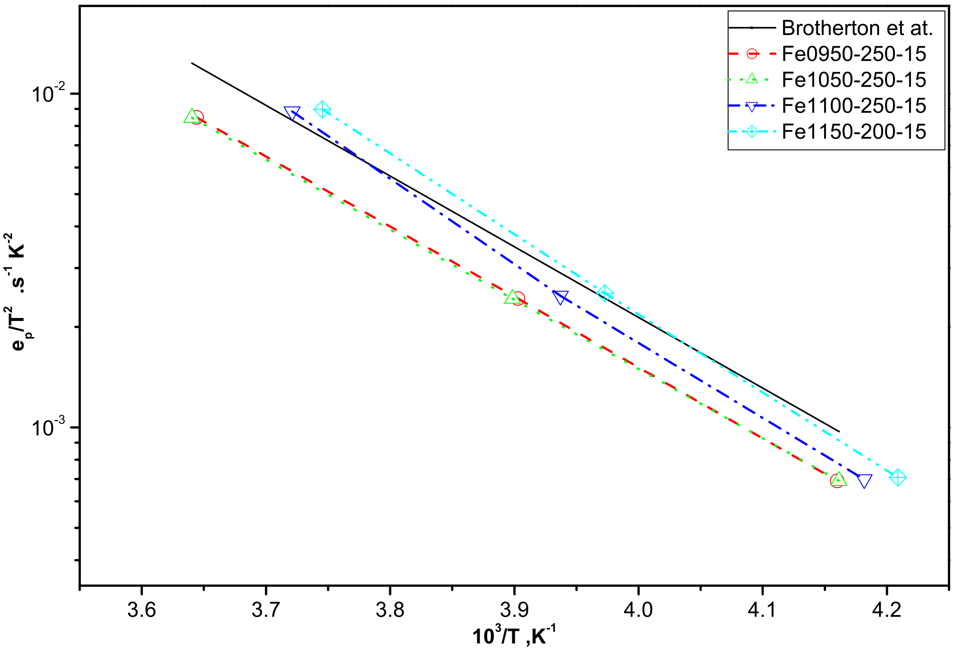

Figure 4.12: Thermal emission rates (T^2 corrected) as a function of inverse temperature for DLTS peaks observed in the samples Fe950-250-15, Fe1050-250-15, Fe1100-250-15 and Fe1150-200-15. The measurement conditions: Filling pulse height $U_\mathrm{p} = 3$ V; filling pulse width 10 μs; reverse bias $U_\mathrm{B} = 3$ V. Also included are the data from Brothertone et al.[16].

It is clearly seen, that the emission rates for the samples, where the iron concentration is lower or equal to the boron concentration (Fe950-250-15 and Fe1050-250-15), coincide and the energy levels are close to the value obtained by Brotherton et al. but with somewhat different prefactors. While at iron concentrations approximately equal or higher than the boron doping level (Fe1100-250-15 and Fe1150-200-15), the emission characteristic still fall into the range measured by different groups for $\mathrm{Fe_i}$, but the energy levels appear to be slightly deeper than for previous samples with smaller iron concentration.

The energy levels and capture cross sections calculated for ”$\mathrm{Fe_i}$-clusters” in different samples are presented in Table 4.1. The Table also included the data for isolated $\mathrm{Fe_i}$ obtained by Brotherton et al..

Sample	E_T, (eV)	σ^* (10^{-16}) cm^2	c_{Fe} $(10^{15}$ cm$^{-3})$
Brotherton et al.	0.42	2.70	?
Fe0950-250-15	0.40	0.69	0.13
Fe1050-250-15	0.42	1.40	1.13
Fe1100-250-15	0.46	14.0	2.88
Fe1150-200-15	0.47	23.0	6.90

Table 4.1: The energy levels and capture cross sections of the interstitial iron-clusters line have been calculated for samples Fe0950-250-15, Fe1050-250-15, Fe1100-250-15 and Fe1150-200-15. Also included is the value from Brotherton et al..

The Capture kinetics of "Fe_i-clusters" for samples with different Fe concentration

The relation between the DLTS-line amplitude $\Delta C_{max}/C_o$ and the filling pulse width t_p establishes the capture characteristics of a defect. For the isolated Fe_i-donor ($E_{Fe} = E_V + 0.42$ eV, $\sigma_p = 2.7 \times 10^{-16}$ cm^{-2}) in p-type silicon ($N_D = 1 \times 10^{15}$ cm^{-3}), t_p-values well below 1μs are needed to observe the exponential filling kinetics ($\Delta C_{max} \sim [1 - \exp(-c_p p t_p)]$; $c_p = \sigma_p < v_{th} >$ and v_{th} is the thermal velocity of holes) usual for point defects. For $t_p = 1$ μs, about 90% of the Fe_i donors are already occupied by holes at the end of refilling pulse. Within the t_p-range of our experiments (1 to 100 μs), point defects having capture cross section $\sigma_p \geq 10^{-16}$ cm^2 are expected to show only minor changes of the line amplitude with t_p-variation.

For extended defects with localized states the situation is rather different. As we have seen in Figures (4.6-A, 4.8, 4.9-A and 4.10-A), Fe_i-clusters show the logarithmic capture kinetics $[(\Delta C_{max}) \sim \ln(t_p)]$, typical for all extended defects with localized states.

The variation of capture characteristics with variation of Fe concentration can be used to obtain some information about evolution of cluster size. Let f_T is a fraction of occupied Fe$_\mathrm{i}$-cluster states, $f_\mathrm{T} = \frac{n_\mathrm{T}^+}{N_\mathrm{T}}$, where n_T^+ is the concentration of cluster states, which are filled with holes, and have been calculated from the measured $\Delta C/C_o$-values. Let us assume that the total number of states in clusters is equal to the iron concentration. Then have $f_\mathrm{T} = \frac{n_\mathrm{T}^+}{c_\mathrm{Fe}}$. The logarithmic dependence of f_T on t_p indicates the existence of the capture barrier $E_\mathrm{cap} \approx \alpha f_\mathrm{T}$ caused by electric charge of the cluster. Since the Fe-clusters have with very narrow energy spectrum the capture term in kinetic equation is quite simple:

$$\frac{df_\mathrm{T}}{dt} = p\sigma v_\mathrm{th}\left(1 - f_\mathrm{T}\right)\exp\left(\frac{-\alpha f_\mathrm{T}}{k_\mathrm{B}T}\right) - e_\mathrm{p} f_\mathrm{T} \tag{4.1}$$

where p is a concentration of free holes.

We can neglect the emission term since the capture is much faster than emission in a condition of DLTS measurement (as long as t_p is much shorter than a DLTS correlation time). From our experimental data we see that $f_\mathrm{T} \ll 1$. Then the Equation 4.1 can be easily solved and we have:

$$f_\mathrm{Fe} = \frac{k_\mathrm{B}T}{\alpha}\ln\left(\frac{t_\mathrm{p}}{t_\mathrm{p}^*}\right) \tag{4.2}$$

where

$$t_\mathrm{p}^* = \frac{1}{p\sigma v_\mathrm{th}} \tag{4.3}$$

Figure 4.13 represents this capture characteristic for the samples with various iron concentrations. In this Figure the fraction of occupied Fe$_\mathrm{i}$-cluster states f_T are shown in a semi-logarithmic plot depending on $\ln(t_\mathrm{p})$ for various iron concentration in the range from 1.3×10^{14} to 6.9×10^{15} cm^{-3}. One can see in Figure 4.13 that for all c_Fe, the f_T depends linearly on $\ln(t_\mathrm{p})$ with a slope depending on c_Fe. The slope contains the information not only about total number of states in clusters, but also about Coulomb capture barrier at the clusters.

The values of t_p^* obtained from a fits of experimental data, shown in Fig. 4.13 by Equation 4.2 gives approximately the same value of parameter $t_\mathrm{p}^* = 3.6 \times 10^{-7}$sec. The capture cross-section calculated from this t_p^* using Equation 4.3 was found of

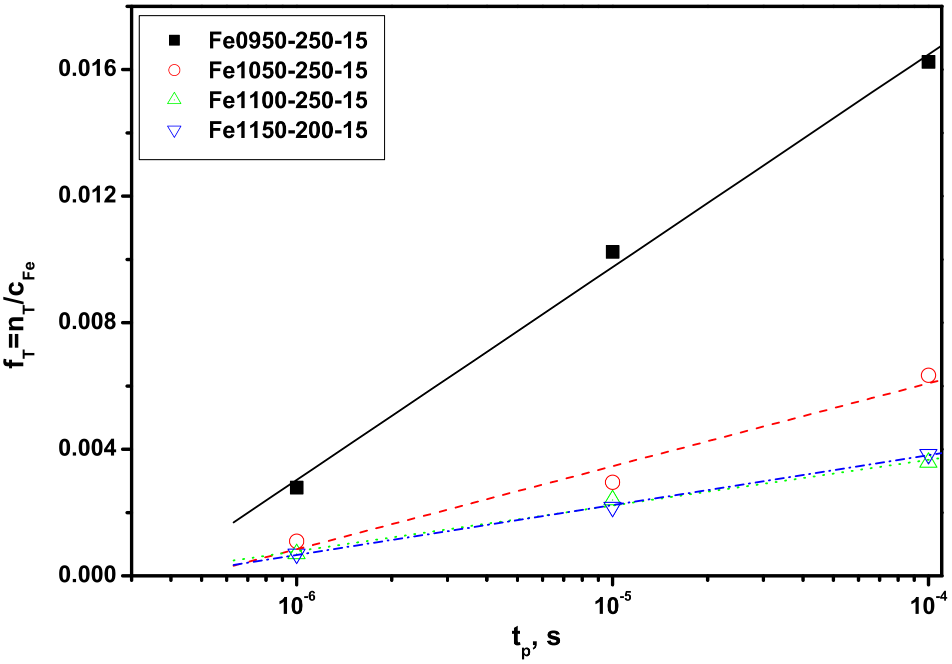

Figure 4.13: Concentration of filled deep levels n_{T}^{+}, as a function of the filling time t_{p} for iron-clusters defect. $U_{\mathrm{B}} = U_{\mathrm{p}} = 3$ V, $T_{\max} = 240$ K, $f = 17$ Hz..

about $\sigma = 1.5 \times 10^{-16}\mathrm{cm}^2$, that is in a good agreement with the values of σ obtained from emission characteristics (see Table 4.1).

The coefficient α is related only to the shape and size of the $\mathrm{Fe_i}$-cluster, and to concentration ρ^* of Fe inside cluster. Points in Figure 4.14 shows the dependence of α on c_{Fe}, calculated from slopes of lines, shown in Figure 4.13.

Two theoretical curves shown in Figure 4.14 are calculated for two extreme cases:

(i) Curve "1" is calculated under assumption, that cluster parameters (size, shape and ρ^*) do not depend on Fe concentration in sample, so that with increasing of c_{Fe} only the concentration ρ of clusters is increasing.

(ii) Curve "2" is calculated for another extreme case: we have assumed that the concentration ρ of clusters is constant (as well as ρ^*). We assume for simplicity that clusters are spherical. Then the radius 'r' of cluster must increase with

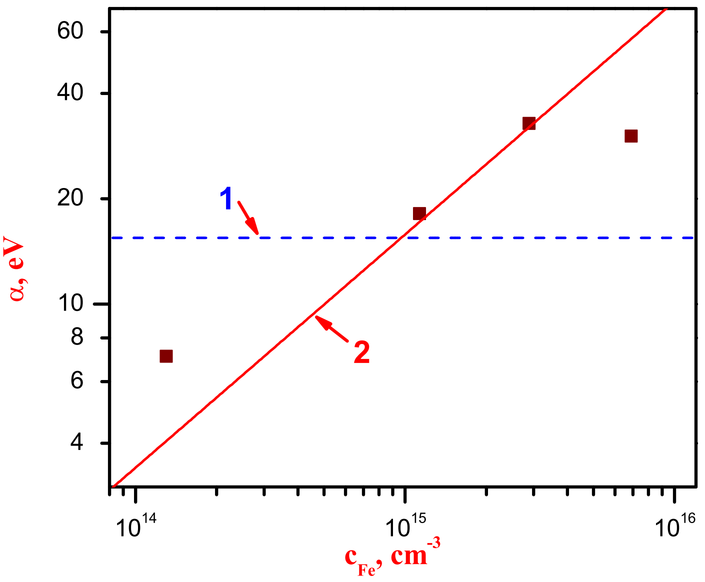

Figure 4.14: A dependence of coefficient α on iron concentration c_{Fe}, calculated from data presented in Figure 4.13 ($\alpha = kT/\left(d(n_{\mathrm{T}}/c_{\mathrm{Fe}})/d\left(\ln\left(t_{\mathrm{p}}\right)\right)\right)$. Curve (2) is calculated for constant ρ and ρ^* (for calculation we used $\rho^* = 5 \times 10^{21}\mathrm{cm}^{-3}$ and $\rho = 3.9 \times 10^{10}\mathrm{cm}^{-3}$).

increasing of c_{Fe} like

$$r = \left(\frac{3c_{\mathrm{Fe}}}{4\pi\rho\rho^*}\right)^{1/3}.$$

The Coulomb barrier around cluster can be calculated as following:

The electric charge 'q' of a cluster is given by

$$q = \frac{e f_{\mathrm{Fe}} c_{\mathrm{Fe}}}{\rho}.$$

Since in our experimental conditions $E_{\mathrm{cap}} \approx \alpha f_{\mathrm{T}} \gg kT$ we can neglected for simplicity the Debye tail in a screening, so that the screening radius R_{sc} is just

$$R_{\mathrm{sc}} = \left(\frac{3q}{4\pi p}\right)^{1/2} \tag{4.4}$$

The electric field E around of spherical cluster can be then written as:

$$E(R) = \left(\frac{1}{eR^2}\right)\left(q - \frac{4}{3}\pi R^3 p\right) \tag{4.5}$$

The Coulomb bend bending $E_{\mathrm{cap}} \approx \alpha f_{\mathrm{Fe}}$ and value of $\alpha = dE_{\mathrm{cap}}/df_{\mathrm{Fe}}$ can be found by integration of Equation 4.5 over R from r to R_{sc}. Curve (2) in Figure 4.14 was calculated using these formulas. There are only two unknown parameters, necessary for calculation of theoretical dependence $\alpha(c_{\mathrm{Fe}})$- values of ρ and ρ^*. These two parameters are dependent on each other and only one of these two parameters can be obtained by the fit. Assuming that $\rho^* = 5 \times 10^{21}$ cm^{-3} we have from a fit $\rho = 3.9 \times 10^{10}$ cm^{-3}.

One can see from Figure 4.14, that the experimental data are in some way between the theoretical predictions (i) and (ii). So, we conclude, that with increasing iron concentration, the size of clusters is growing, and, in addition, the concentration of clusters probably also increases. To make more detailed conclusions one need some more experimental data.

The main feature of the localized state model is that after normalization of the line amplitudes the high-T sides of the lines for different filling pulse duration coincide. Figure 4.15 illustrates this coincidence for the DLTS-line associated with samples Fe950-250-15, Fe1050-250-15, Fe1100-250-15 and Fe1150-200-15.

It follows from the figure that the high-temperature sides for each sample coincide, i.e. the defect states are localized. The low-temperature sides reveal, that the DLTS-line of $t_{\mathrm{p}} = 1$ μs is broader than the DLTS-line with higher filling pulse duration, but this can be resulted from the presence of some other point defects with small (about 10^{12} cm^{-3}) concentration.

4.3 Transition from $\mathrm{Fe_i}$-clusters to iron silicide precipitates

We are not aware of any iron silicide phase, whose electronic properties resemble to those of the $\mathrm{Fe_i}$-clusters, so that these clusters are not expected to be a stable phase in the Fe-Si system. Indeed, as we show in this section, the $\mathrm{Fe_i}$-cluster is a metastable precursor of another iron precipitate, which either directly evolves

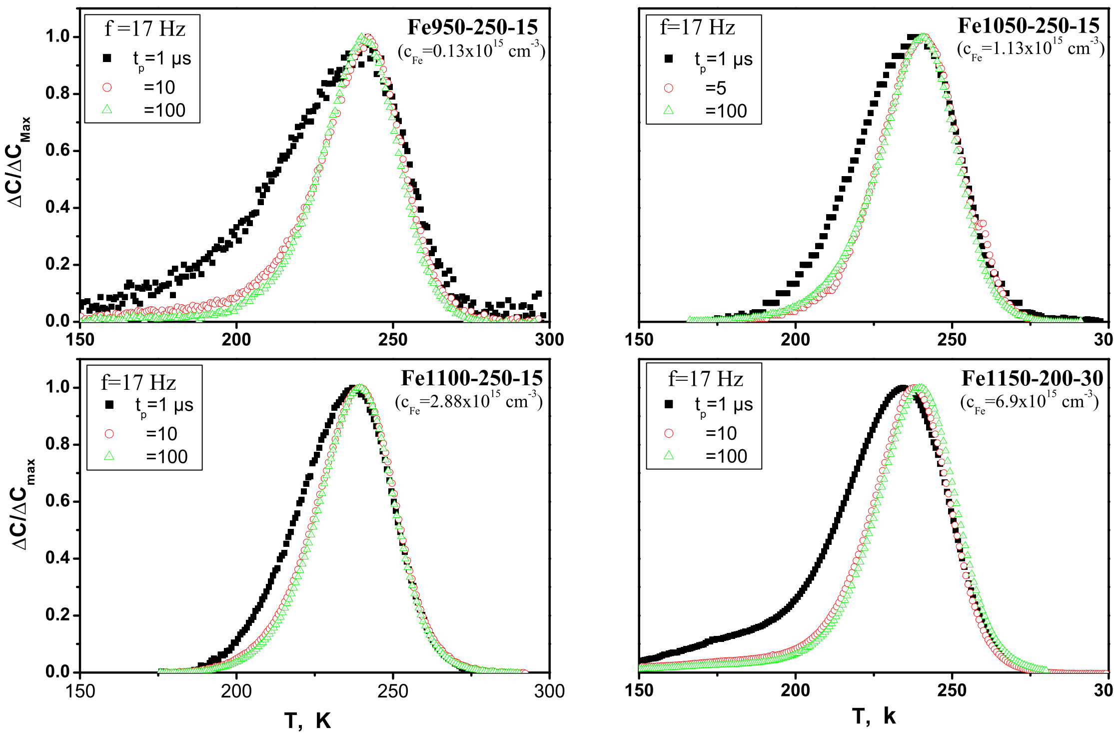

Figure 4.15: Filling pulse width evaluation of the DLTS-line associated with samples Fe950-250-15, Fe1050-250-15, Fe1100-250-15 and Fe1150-200-15. For better comparison, the different spectra are normalized.

from the Fe_i-cluster by an internal transformation or which nucleates and grows in competition with the Fe_i-cluster. The electronic properties of the iron precipitates are significantly different from those of the Fe_i-cluster and resemble those of small Cu-and Ni-silicide precipitates in silicon. Within the ranges of the in-diffusion temperatures (950 - 1200°C), annealing temperatures (200 - 250°C) and times (15 and 30 minutes), covered in our experiments, we observe only Fe_i-clusters for $T_D \leq 1050°C$ ($c_{Fe} = 1.13 \times 10^{15}$ cm^{-3}), Fe_i-clusters and Fe-precipitates for $T_D = 1100°C$ ($c_{Fe} \leq 2.9 \times 10^{15}$ cm^{-3}) and only Fe-precipitates for $T_D = 1200°C$ ($c_{Fe} \leq 1.6 \times 10^{16}$ cm^{-3}). The phase of the iron precipitate has not been yet identified. We have found it unchanged on annealing at 550°C for 15 minutes and therefore presume that it is one of the iron silicide phases (see discussion).

4.3.1 The characterization of the DLTS of iron-precipitates

Typical DLTS spectra, obtained after iron in-diffusion at 1100°C and subsequent annealing at 200°C for 30 minutes, are presented in Figure 4.16.

The "interstitial iron-clusters" line, which was studied in the previous sections and which we attributed to Fe$_i$-cluster with localized states, is not detectable anymore. Instead a new significantly broadened line has appeared. Compared to Fe$_i$-cluster line, this new line has strongly reduced the amplitude and has different behaviour of the DLTS line shape and amplitude with variation of t_p, namely typical for the bandlike states[47].

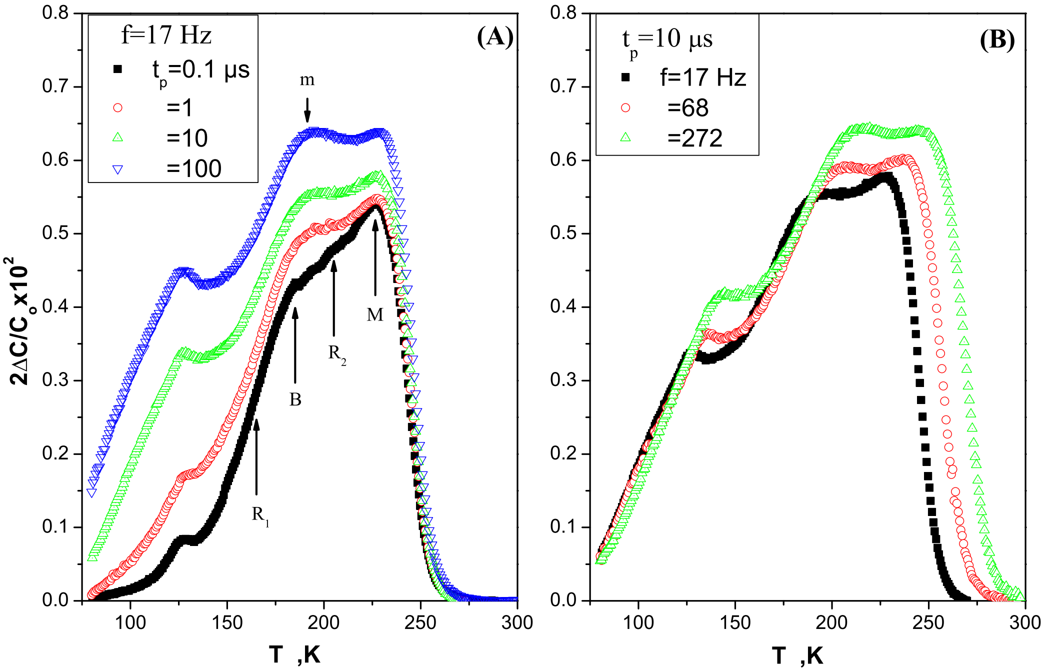

Figure 4.16: DLTS spectra after iron was in-diffused at 1100°C for 35 minutes and annealed at 200°C for 30 minutes. The measurement conditions are (A) Filling pulse duration of 0.1, 1, 10 and 100 μs at frequency $f = 17$ Hz. (B) Repetition frequency of 17, 68 and 272 Hz at filling pulse duration $t_p = 10$ μs. The filling pulse height $U_p = 3$ V and the bias voltage $U_B = 3$ V.

Figure 4.16-A shows the variation of the line with increasing filling pulse length t_p, i. e. the capture characteristics. The line shape obtained for $t_p = 0.1$ μs is described by a steep rise on the low-T side (R$_1$), a break (B), a second but less steep rise

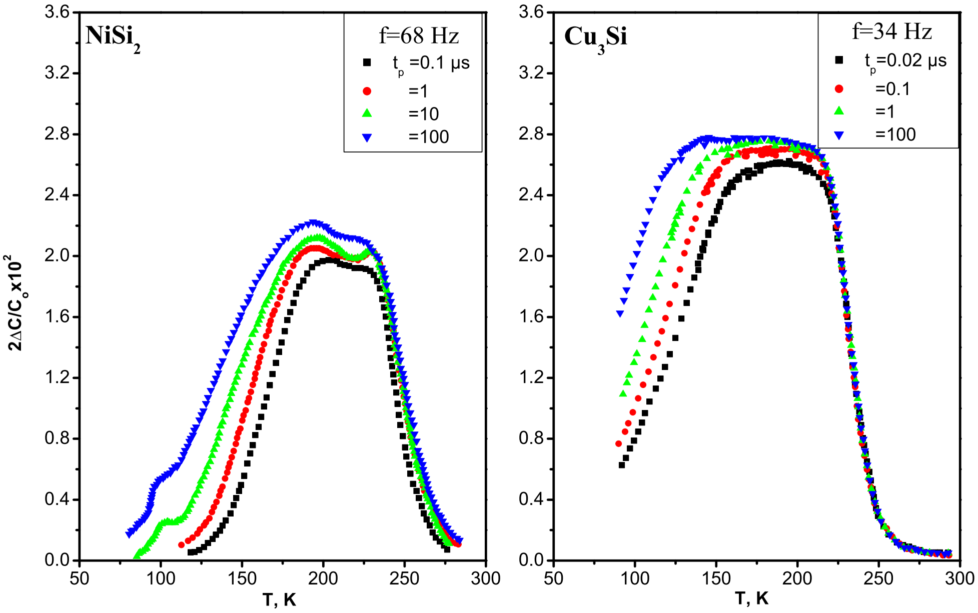

Figure 4.17: DLTS spectra for nickel silicide and copper silicide precipitations as examples of the DLTS spectra box-like shape. DLTS spectra for $NiSi_2$[56] and Cu_3Si[66] after Ni and Cu were in-diffused in n-type silicon at 750°C, respectively. The measurement conditions for $NiSi_2$ are: filling pulse durations of 0.1, 1, 10 and 100 μs at frequency 68 Hz. The filling pulse height $U_\mathrm{p} = 4$ V and the bias voltage $U_\mathrm{B} = 4$ V. For Cu_3Si are: filling pulse durations of 0.02, 0.1, 1 and 100 μs at frequency 34 Hz. The filling pulse height $U_\mathrm{p} = 4$ V and the bias voltage $U_\mathrm{B} = 4$ V.

(R_2) and a maximum (M) just below the high-T side. The low-T side R_1 shows a maximum which as we will see below results from the superposition of an additional line associated to a point defect. With increasing t_p, the maximum M keeps its position on the T-axis and the high-T sides coincide. The main change consists of a continuous decrease of the slope of R_2, possible by a gradual development of a second maximum (m) at the position of the break B. For $t_\mathrm{p} = 100$ μs the line ascribed to the Fe-precipitate has the shape of a trapezoid. A similar line shape has been observed for $NiSi_2$-precipitates[56] and for Cu_3Si-precipitates[66] in n-type silicon after quenching from a diffusion temperature of 750°C (Figure 4.17) and it has been attributed to the box-like density of states spectrum for electronic energy band of precipitate.

We should mention that the precipitates of Cu and Ni have been observed and identified by TEM, which so far is not the case for the Fe-precipitates.

In the model of bandlike states[47, 65], increasing of filling pulse duration t_p results in broadening of DLTS line by growing of the low temperature part of line, while the high-temperature sides of line coincide for different t_p. It has been shown by simulations[65] and analytical calculations[55], that this kind of behaviour is a fingerprint of bandlike states. Applying the above criteria on the spectra presented in Figure 4.16 clearly shows that the Fe-precipitate introduce bandlike states.

DLTS measurements using different frequencies (Figure 4.16-B) reveal, that the high-temperature sides of the DLTS-lines shift along the temperature axis to higher temperatures with increasing correlation frequency, while at the low-temperature sides of R_1, the spectra coincide (independent on the frequency). A similar behaviour has been observed previously for copper precipitates in n-Si[30, 66]. One needs a sophisticated computer modelling to analyse obtained DLTS spectra and to find the density of states and other parameters of precipitates. So far this kind of analysis is still missing.

4.3.2 Dependence of DLTS of Fe-precipitates on iron concentration

In this section we study the effect of the diffusion temperature, i.e. that of iron concentration, and of the formation temperature on the DLTS line shape and on the capture and emission characteristics of the Fe-precipitate.

Figures 4.18, 4.19, 4.20 and 4.21 show typical DLTS spectra observed for samples, which were annealed at 200 and 250°C for 15 and 30 minutes after in-diffusion of iron at 1200°C for 20 minutes ($c_\mathrm{Fe} = 1.6 \times 10^{16}$ cm^{-3}).

One observes that the DLTS spectra show essentially the same behaviour as for

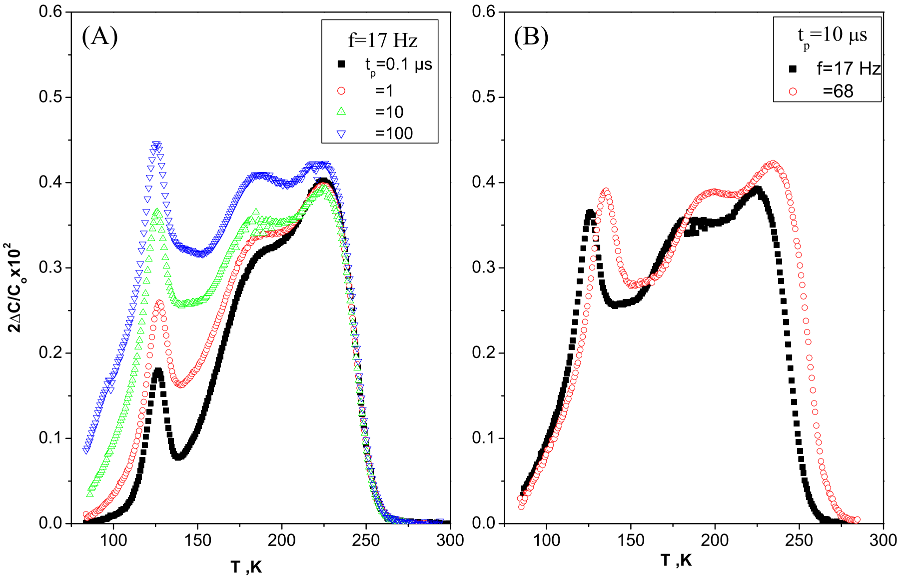

Figure 4.18: DLTS spectra for sample Fe1200-200-15. The measurement conditions are (A) Filling pulse duration of 0.1, 1, 10 and 100 μs at frequency $f = 17$ Hz. (B) Repetition frequency of 17 and 68 Hz at filling pulse duration $t_\mathrm{p} = 10$ μs. The filling pulse height $U_\mathrm{p} = 3$ V and the bias voltage $U_\mathrm{B} = 3$ V.

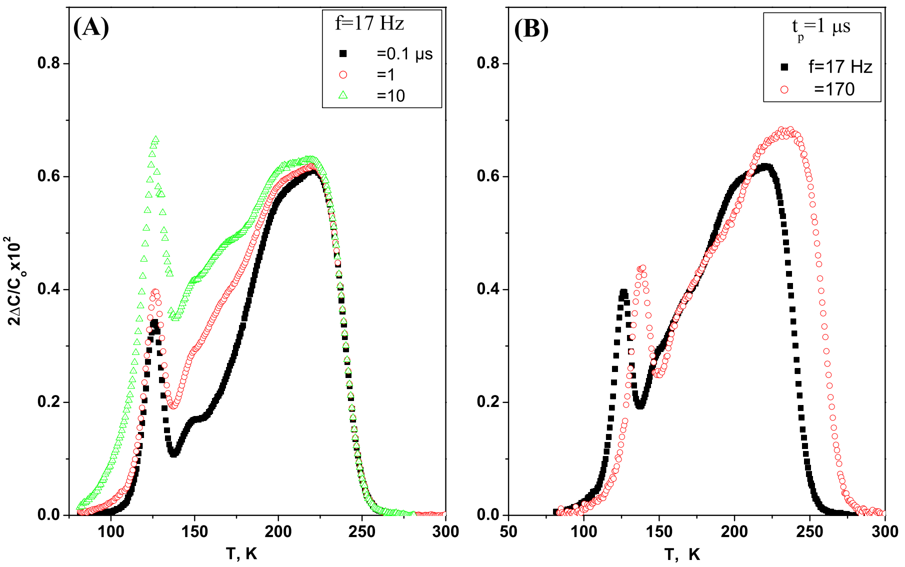

Figure 4.19: DLTS spectra for sample Fe1200-200-30. The measurement conditions are (A) Filling pulse duration of 0.1, 1 and 10 μs at frequency $f = 17$ Hz. (B) Repetition frequency of 17 and 170 Hz at filling pulse duration $t_\mathrm{p} = 1$ μs. The filling pulse height $U_\mathrm{p} = 3$ V and the bias voltage $U_\mathrm{B} = 3$ V.

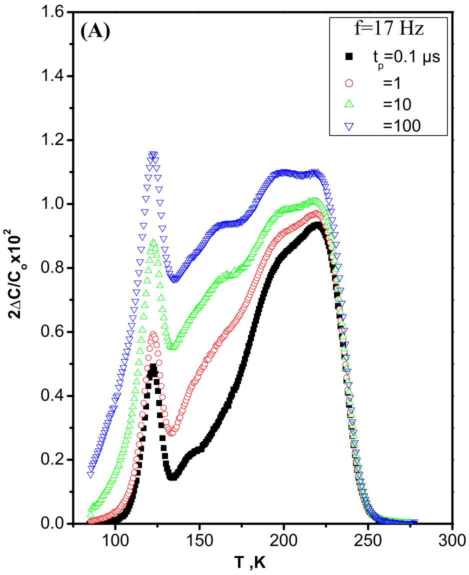

Figure 4.20: DLTS spectra for sample Fe1200-250-15. The measurement conditions are (A) Filling pulse duration of 0.1, 1, 10 and 100 μs at frequency $f = 17$ Hz. (B) Repetition frequency of 17, 68 and 272 Hz at filling pulse duration $t_{\mathrm{p}} = 10$ μs. The filling pulse height $U_{\mathrm{p}} = 3$ V and the bias voltage $U_{\mathrm{B}} = 3$ V.

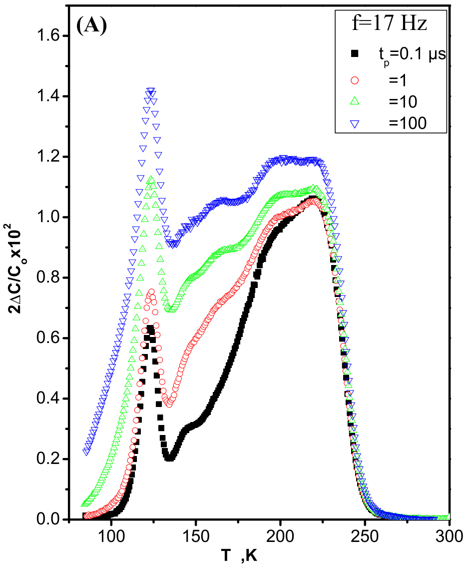

Figure 4.21: DLTS spectra for sample Fe1200-250-30. The measurement conditions are (A) Filling pulse duration of 0.1, 1, 10 and 100 μs at frequency $f = 17$ Hz. (B) Repetition frequency of 17, 68 and 272 Hz at filling pulse duration $t_{\mathrm{p}} = 10$ μs. The filling pulse height $U_{\mathrm{p}} = 3$ V and the bias voltage $U_{\mathrm{B}} = 3$ V.

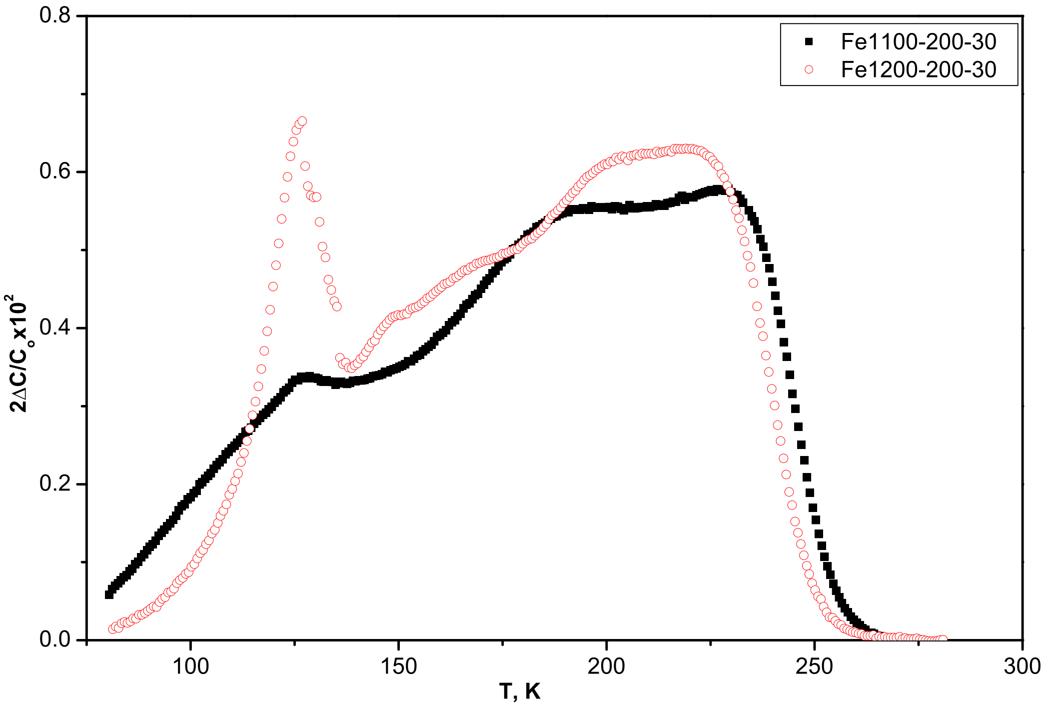

Figure 4.22: The effect of iron concentration on the DLTS-spectra of samples iron was in-diffused at temperatures 1100 and 1200°C and subsequent the samples were annealed at 200°C for 30 minutes. The measurement conditions are filling pulse duration of 10 μs and the repetition frequency of 17 Hz.

the sample Fe1100-200-30 (Figure 4.16-A). Applying the above criteria it is clearly shown that the DLTS-line defect introduce bandlike states.

The comparison between the two samples Fe1100-200-30 and Fe1200-200-30 which were annealed at the same temperature and time are shown in Figure 4.22. Increasing the diffusion temperature from 1100 to 1200°C means a change of the iron concentration from $c_{\mathrm{Fe}} = 2.9 \times 10^{15}$ to 1.6×10^{16} cm^{-3}. At the same time, as one can see in Figure 4.22, the DLTS-line shape and even amplitude remain qualitatively the same. Apparently the structural unit of the precipitate which generates the deep electronic states do not drastically change with iron concentration.

The main difference between two spectra in Figure 4.22 is the amplitude of the DLTS line on the low-temperature sides of iron precipitate line. One can see that with increasing T_{D} there is a significant increase of its amplitude. This line can be as-

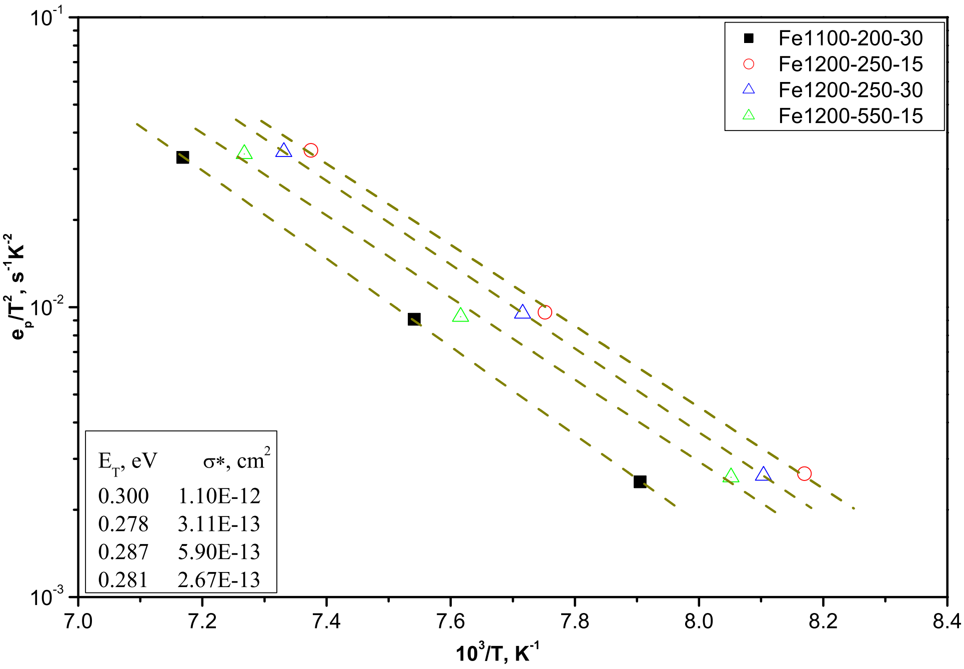

Figure 4.23: Arrhenius plots for point defect line for samples Fe1100-200-30, Fe1200-250-15, Fe1200-250-30 and Fe1200-550-15 with different iron concentrations, annealing temperatures and times.

sociated with some point defect. Its emission characteristics are given in Figure 4.23.

Figure 4.24-A and 4.24-B shows the dependence of DLTS line of Fe-precipitates on the annealing parameters. One can see that the line amplitude depends on the annealing time and temperature stronger than on initial iron concentration. It increases with increasing of annealing temperature and time. However, the shape and the width of the line do not depend strongly on these parameters.

The effect of annealing at higher temperature

To identify the structural units which generate deep electronic states of a precipitate in the band-gap, annealing experiments at temperatures at which internal ripening starts have been proven very useful for $NiSi_2$- and for Cu_3Si-precipitates.

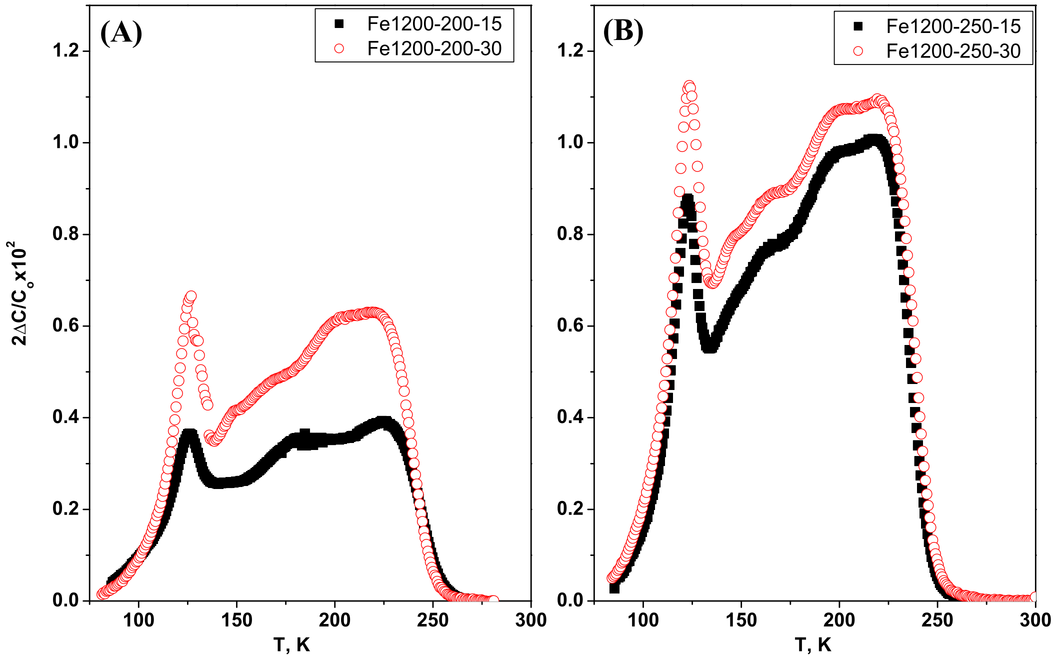

Figure 4.24: The effect of the annealing temperatures and annealing times on the DLTS-spectra for samples iron was in-diffused at temperature 1200°C. The measurement conditions are filling pulse duration of $t_{\mathrm{p}} = 10$ μs and the repetition frequency of $f = 17$ Hz. The filling pulse height $U_{\mathrm{p}} = 3$ V and the bias voltage $U_{\mathrm{B}} = 3$ V.

In case of $NiSi_2$- and Cu_3Si-precipitates, during quenching from diffusion temperature the solid solution of Cu or Ni in silicon becomes very highly supersaturated and this results in generation of some metastable precipitates. $NiSi_2$-precipitates have been studied by high resolution transmission electron microscopy (HRTEM). They were found to be platelets consisting of two (111) $NiSi_2$-planes. The structural units are the interface to the silicon bulk with of Si-Si bonds along the (111)-planes and sevenfold coordinated Ni-atom (instead of eightfold in the bulk) and a dislocation with four-, five- and six-fold coordinated Ni-atoms in its core that borders the platelet.

On annealing at temperatures between 250°C and 320°C, the thin platelet undergoes a transformation of shape into a thicker one without appreciable long range diffusion to other platelets. The simultaneous study of this "internal ripening", as

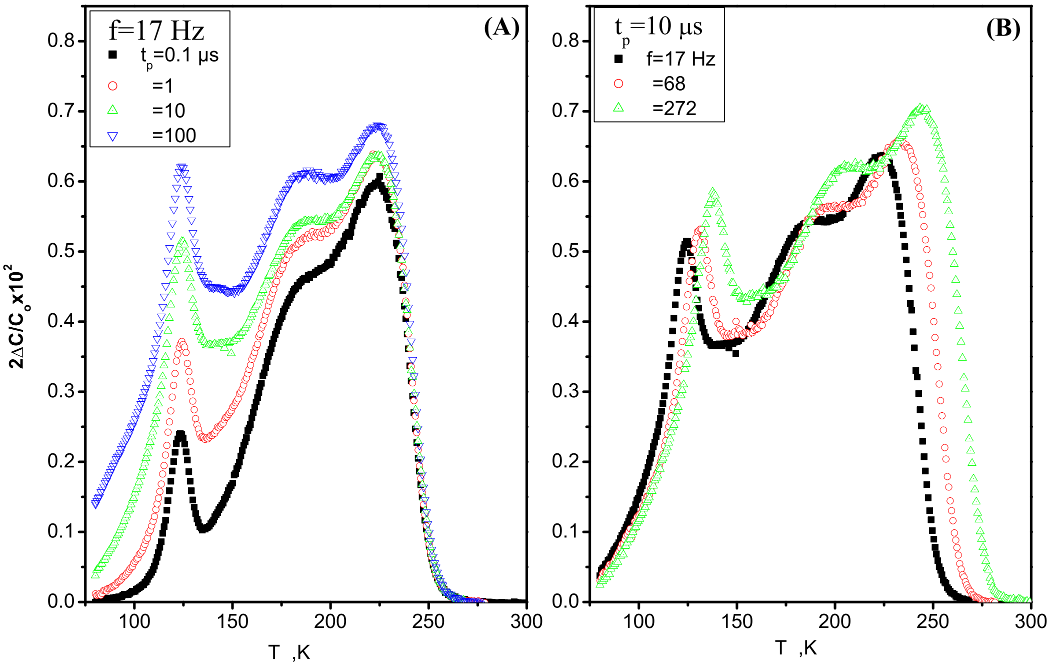

Figure 4.25: DLTS spectra for sample Fe1200-550-15. The measurement conditions are (A) Filling pulse duration of 0.1, 1, 10 and 100 μs at frequency $f = 17$ Hz. (B) Repetition frequency of 17, 68 and 272 Hz at filling pulse duration $t_{\mathrm{p}} = 10$ μs. The filling pulse height $U_{\mathrm{p}} = 3$ V and the bias voltage $U_{\mathrm{B}} = 3$ V.

it has been called, by DLTS and HRTEM has shown, that the measured DLTS-line is caused by the dislocation bounding the platelet. The character of its density of states changes from bandlike to localized states at the onset of internal ripening. A similar transformation of shape has been observed for thin Cu_3Si-platelets on annealing at 260°C. However, in this case the density of states remained bandlike. Therefore, it has been associated to the Si/Cu_3Si interface.

Obviously, it was interesting made an attempt to investigate the influence of internal ripening to the DLTS line of iron precipitates. To approach the conditions similar to condition of internal ripening for the $NiSi_2$-platelets, we have chosen an annealing at 550°C for 15 minutes to form Fe-precipitates from the supersaturated solution, see Figure 4.25.

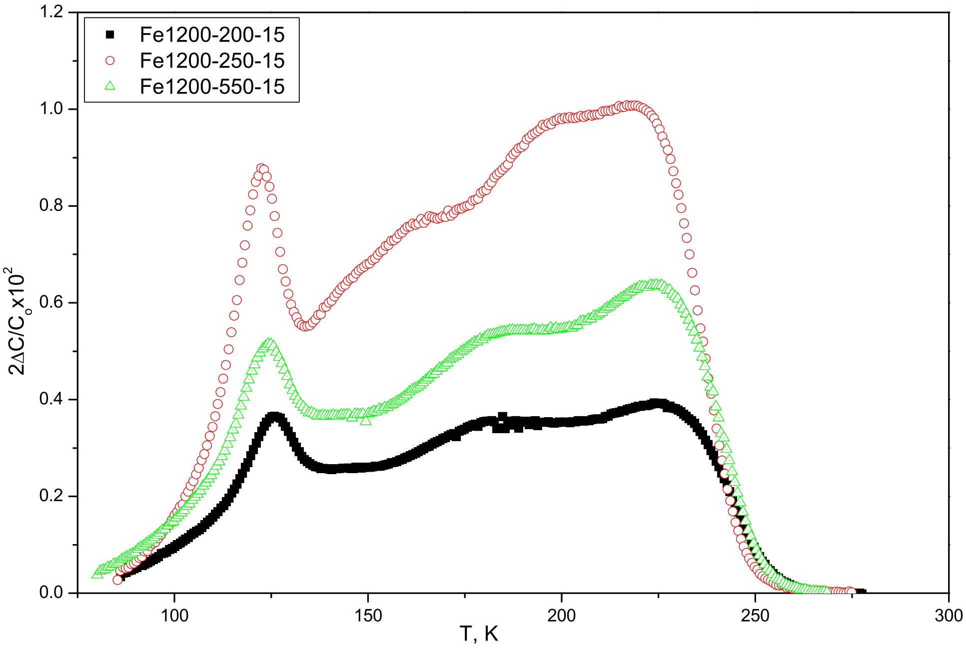

Figure 4.26: Effect of annealing temperature on the DLTS lines amplitude for iron-doped Si $\sim 1.56 \times 10^{16}$ cm^{-3} for samples Fe1200-200-15, Fe1200-250-15 and Fe1200-550-15. The measurement conditions are the filling pulse duration of 10 μs and the frequency 17 Hz. The filling pulse height $U_\mathrm{p} = 3$ V and the bias voltage $U_\mathrm{B} = 3$ V.

Extrapolated solubility and diffusivity of iron at 550°C (1.9×10^8 cm^{-3}; 9×10^{-8} cm^2/s) are close to the values for nickel at 260°C (1.6×10^8 cm^{-3}; 7×10^{-8} cm^2/s). It is therefore expected that formation as well as internal ripening of Fe-precipitates take place during annealing.

Figure 4.25 shows the DLTS spectra sets for different t_p and frequencies measured for Fe-precipitates formed at 550°C, while Figure 4.26 shows for comparison the DLTS-lines of Fe-precipitates, formed at 200, 250 and 550°C. One can see that the annealing at 550°C did not result in any dramatic change of characteristics of DLTS line. The character of their density of states remains bandlike as in the case of Cu_3Si-precipitates and opposite to the case of $NiSi_2$-precipitates. Therefore, the electronic states of Fe precipitates are more probably related to the surface or to the volume of precipitate rather than to any bounding dislocation, as it was observed for $NiSi_2$-precipitates.

Chapter 5

Discussion and Summary

5.1 Discussion

We have presented a deep level transient spectroscopy (DLTS) study of the evolution of iron point defects into clusters and precipitate defects in iron-doped p-type silicon. DLTS measurements are used to identify the electrically active defects produced by iron at concentration levels from 1.3×10^{14} to 1.56×10^{16} cm^{-3}. Analyses of DLTS results obtained in samples annealed in the temperature range 200 - 550°C allow us to monitor the transition from simple point defects (isolated $\mathrm{Fe_i}$ and FeB pairs) to $\mathrm{Fe_i}$-clusters and to Fe-precipitate defects that occur upon increasing the iron concentration and annealing temperature. The application of recently developed criteria for the interpretation of DLTS spectra from extended defects allowed to concluding that deep electronic states associated with the $\mathrm{Fe_i}$-clusters have localized states and the Fe-precipitates most likely have bandlike states character.

Collins and Carlson[67] have proved the interstitial iron level and suggested the possibility of pairing of iron with boron. Ludwig and Woodbury[68, 69] have succeeded to detect the FeB-pair by EPR and Feichtinger[70] has identified the energy level of iron interstitial and FeB-pair levels of $(E_\mathrm{V} + 0.4 \pm 0.05)$ eV and $(E_\mathrm{V} + 0.1 \pm 0.01)$ eV, respectively, from Hall effect studies. That was later confirmed by a number of Hall effects and DLTS studies of various research groups.

We doped dislocation-free p-type FZ silicon [$c_\mathrm{B} = 1 \times 10^{15}$ cm^{-3}] samples by iron in-diffusion at different temperatures, followed by fast quenching. When the total concentration of Fe is smaller than of B-atoms, subsequent sample storage at room temperature eliminates isolated $\mathrm{Fe_i}$ atoms almost completely by their transformation to FeB pairs. The concentration of the FeB-pair estimated from measured amplitude of the ($E_\mathrm{V}+0.1$ eV)-DLTS-line is very close to the value calculated from known solubility of Fe at 950°C. During annealing at 200°C for 30 minutes the DLTS-line amplitude of FeB decreases whereas that of $\mathrm{Fe_i}$ increases. This behaviour is in agreement with literature data and has been attributed to the dissociation of FeB-pairs into $\mathrm{Fe_i^{(+)}}$ and $\mathrm{B^{(-)}}$.

Clustering of transition elements in silicon has been studied since 1959, but so far limited to small clusters of up to two or four interstitial atoms. Ludwig et al.[68] were the first to detect the EPR spectrum of a $\mathrm{(Mn_i)_4^0}$-cluster with four neutral $\mathrm{Mn_i}$-atoms positioned in the corners of a regular tetrahedron.

In 1982 an EPR-spectrum associated with pairs of interstitial iron $\mathrm{(Fe_i)_2^+}$ was found by Muller et al.[26]. Its intensity was maximal directly after quenching from high temperatures and disappeared on storage at room temperature after 12 hours or on annealing at 75°C after 1 hour. It is generally agreed that the disappearance of this EPR centre is caused by agglomeration of further $\mathrm{Fe_i}$ leading to larger clusters.

A trigonal EPR spectrum, starting to appear on annealing at 120°C and reaching its maximum intensity on annealing around 140°C, has been associated with $\mathrm{(Fe_i)_4^0}$ and modelled by four ferromagnetically coupled spins $S = 1$ of $\mathrm{Fe_i^0}$ yielding an effective spin of the cluster of $S = 4$.

The formation of $\mathrm{(Fe_i)_4}$ was found strongly related to the decrease of the $\mathrm{Fe_i}$-concentration, beginning at 120°C. Above 140°C, when the $\mathrm{Fe_i}$-concentration has reduced to about half of its initial value, a part of the $(\mathrm{Fe_i})_4$-clusters disappears, another one survives to temperatures of 200 to 250°C. The authors argue that the first drop occurs when interstitial iron agglomerates to Fe-clusters and makes them grow, while for the second drop $(\mathrm{Fe_i})_4$-clusters first dissociate to form larger clusters.

The formation of $\mathrm{Fe_i}$-clusters investigated by us may be seen as a continuation of this scenario. The cluster $(\mathrm{Fe_i})_4$ disappears in about the same temperature range in which the $\mathrm{Fe_i}$-cluster giving rise to the "cluster"-line we found in DLTS are formed. Since the shortest annealing time in our experiments is 15 minutes, it is possible that $(\mathrm{Fe_i})_4$ is followed by some "discrete" clusters $(\mathrm{Fe_i})_\mathrm{n}$ with $n > 4$, before the $\mathrm{Fe_i}$-cluster detected by us are generated. The term "discrete" refers to the electrical properties of these clusters. While the $\mathrm{Fe_i}$-cluster investigated by us shows the DLTS-features of a continuous density of localized states, $(\mathrm{Fe_i})_4$ is expected to give rise to a set of separate levels within the band gap of silicon. Although not verified for $(\mathrm{Fe_i})_4$, DLTS[71] and photo-EPR[72] of $(\mathrm{Mn_i})_4$ have shown a donor level near mid-gap at $E_\mathrm{C} - 0.54$ eV and the transition to the double donor $(\mathrm{Mn_i})_4^{++}$ in the lower half of the band-gap. Opposite to what we have found for the $\mathrm{Fe_i}$-cluster, the emission characteristics of $(\mathrm{Mn_i})_4^{(0/+)}$ is distinctly different from those of $\mathrm{Mn_i^{(0/+)}}$ at $E_\mathrm{C} - 0.43$ eV.

In summary, the $\mathrm{Fe_i}$-cluster studied by us with DLTS probably evolves from the discrete $(\mathrm{Fe_i})_4$ observed by EPR, and its discrete successors. At some stage of this development, a qualitative change of the electronic properties must occur, leading from a set of discrete levels to a density of localized states exhibiting the emission characteristics very similar to those of $\mathrm{Fe_i^{(0/+)}}$. Independent of the iron concentration, the cluster defects show logarithmic capture kinetics proving the extended nature of the defects. Assuming that the total number of states of the iron clusters is given by the total iron concentration the dependence of the slope kT/α on iron concentration reflects the size of the clusters. Using a simple approximation for spherical clusters experimental data are reproduced. In addition, the capture cross section obtained from the capture analysis is consistent with that derived from carrier emission. The present data do not allow, however, to conclude about the shape and density of the clusters. Additional experiments including the investigation of the cluster formation kinetics are needed to clarify this point.

The phase of the iron-precipitate which according to our DLTS-studies gives rise to a bandlike density of states (two or three dimensional), centred in the lower half of the silicon band gap, has not been identified so far. Superimposed to the asymmetrically broadened DLTS-Line of the silicide precipitate, several point defect levels or narrow sets of localised states are observed, most clearly one on the low-temperature side, two other ones higher temperature, but below the high-temperature maximum of the precipitate line, are best seen in the large-amplitude spectra (see Appendix A and B). The defects which are responsible for these levels have not been identified so far.

Assuming that the iron-precipitate is a silicide phase, we want to briefly list the potential phases, i.e. the stable bulk ones and the epitaxially stabilised phases on Si(111) in the Fe-system. We confine to Si(111) as the Si/precipitate interface, since the first stages of Co-, Ni- and Cu-precipitates, which are generated during fast quenching from diffusion temperature, are thin platelets on Si(111)- planes[30, 56].

The stable bulk phases of Co and Ni in equilibrium with their solute in silicon are $CoSi_2$ and $NiSi_2$, respectively, both crystallising in the CaF_2-structure with a rather small lattice mismatch to Si. The silicide phases for iron in equilibrium with Si are α-$FeSi_2$ and β-$FeSi_2$ above and below 915°C[41, 42], respectively. Their structure deviates from the one of CaF_2 and is tetragonal and orthorhombic, respectively, both with an appreciable lattice mismatch to Si(111).

However, under the growth conditions of MBE at a Fe/Si-ratio of 1:2 there exists an unstable phase γ-$FeSi_2$ with CaF_2-structure and according to theoretical work almost lattice-matched to Si.

Two classes of metastable phases which are generated from a highly supersaturated solid solution have been obtained from the study of the first stages of Ni- and Cu-precipitation[73]. Precipitates of the first class survive the competition with nucleation and growth of the stable bulk phase because of their high growth rate, while precipitates of the second class are selected because their formation energy under the strain conditions imposed by the bulk silicon becomes smaller than that of the strained bulk phase. Phases belonging to the second class have been also named ”epitaxially stable phases”[74].

It has been argued that $NiSi_2$-platelets bounded by a dislocation ring belong to the first class, and that, since Cu_3Si has a very large lattice mismatch with Si, the platelet is the shape of lowest strain energy, so that Cu_3Si-platelets might belong to second class. As outlined above, Fe has in its variety metastable silicides of both classes with γ-$FeSi_2$ as possible candidate for first class and with FeSi of CsCl-symmetry for second class.

A quantity, which is particularly relevant for precipitates, is the relative volume change per silicon atom when one formula unit of the silicide is formed,

$$\Delta = \frac{\left(V_{\mathrm{Si}}^{(\mathrm{silicide})} - V_{\mathrm{Si}}^{(\mathrm{Si})}\right)}{V_{\mathrm{Si}}^{(\mathrm{Si})}} \quad [73].$$

While for epitaxial growth the planar fitting between the silicon substrate and the silicide layer has to be achieved, silicide precipitates have to be inserted into the silicon bulk. The value Δ measures the number of intrinsic point defects that are involved when a strain-free silicide precipitate is formed. Without the involvement of point defects, which might occur at low temperatures or for small precipitates, Δ is a measure of the strain field energy and is shape-dependent with a preference for platelets. For example, $\Delta = -1.1 \times 10^{-2}$ for $NiSi_2$ and $\Delta = 1.5$ for Cu_3Si.

From the two candidates of the silicide precipitates, studied by us, the Δ-value of γ-FeSi$_2$ is very small like for NiSi$_2$, while for FeSi in the CsCl-structure it is 0.9. This means that FeSi$_2$-precipitates for their high Δ-value have a significant drawback compared γ-FeSi$_2$ precipitates. Hence, we may speculate that iron-related precipitates observed by DLTS in this work consist of the metastable γ-FeSi$_2$ phase. However, a direct proof by TEM is still missing.

5.2 Summary

Small iron precipitates and also clusters which evolve from a highly supersaturated solution of Fe in p-type Si on annealing have been investigated by using DLTS.

Unlike cobalt, nickel and copper, iron can be kept in solution by fast quenching from high temperatures, but alike those elements it occupies the interstitial sites in silicon. These sites have the same size and symmetry as lattice sites and therefore allow diffusion of $\mathrm{Fe_i}$ down to room temperature.

For iron concentrations c_{Fe} smaller than the concentration of boron, c_{B} (serving as the shallow acceptor dopant), i.e. $c_{\mathrm{Fe}} < c_{\mathrm{B}}$, $\mathrm{Fe_i}$ forms $\mathrm{Fe_i^{(+)}B^{(-)}}$-pairs by reaction with boron. Annealing at 200°C for 30 minutes drives the reaction to a balance, where the two DLTS-lines associated with $\mathrm{Fe_i}$ and FeB-pairs represent comparable concentration of the two species. The parameters determining this reaction including the electronic levels of $\mathrm{Fe_i}$ and FeB-pairs are well-known from detailed investigations by various groups.

On annealing at slightly higher temperatures (250°C, 15 minutes) a new defect is generated out of $\mathrm{Fe_i}$. The DLTS-line of $\mathrm{Fe_i}$ disappears and at its position a new line of significantly smaller amplitude appears. The emission characteristic of this new defect indeed falls into the range which has been measured for $\mathrm{Fe_i}$ in the literature. But different from $\mathrm{Fe_i}$, the new defect has the capture characteristic of an extended defect and it does not react with boron. In our interpretation, the resulting electronic structure of the new defect consists of a compact set of localized states within the band gap of silicon close to the level of $\mathrm{Fe_i}$. We have argued against a silicide precipitate and for a cluster of $\mathrm{Fe_i}$ ("Fe-cluster") to be compatible with these properties. This narrow electronic relation between $\mathrm{Fe_i}$ and $\mathrm{Fe_i}$-cluster is unusual in the sense that it is not met by small clusters of a metal impurities, as was be outlined in the discussion section.

With increasing iron concentration to values $c_{\mathrm{Fe}} > c_{\mathrm{B}}$, according to our DLTS data, another type of Fe-precipitate appears on annealing at 200°C for 30 minutes. Its DLTS-line shape, capture and emission characteristic resemble those of $\mathrm{NiSi_2}$- and $\mathrm{Cu_3Si}$-precipitates, as obtained by fast quenching from high temperatures. Based on this similarity, we have argued that the Fe-precipitate constitutes an iron silicide phase. According to our DLTS results, the electronic energy spectrum of precipitates shows all characteristic features of bandlike states, which extend in the lower half of the silicon band gap. The electronic states have their origin either in the bulk of the precipitate or in the interface between precipitate and silicon. From the comparison with the Si-Co, Si-Ni and Si-Cu system the metastable phases γ-$\mathrm{FeSi_2}$, having the $\mathrm{CaF_2}$-structure like $\mathrm{CoSi_2}$ and $\mathrm{NiSi_2}$, or the FeSi-phase with Cs-Cl-structure are possible candidates.

Appendix A

Multi lines DLTS spectra

In all spectra presented so far for the iron precipitate, the line amplitude $\Delta C/C_o$ in units of $2\Delta C/C_o \times 10^2$ did not exceed the value of 1.2. For significantly longer annealing times (120 minutes at 200 and 250°C), but in one case also for our normal annealing conditions (30 minutes at 200°C, $T_{\mathrm{D}} = 1150$°C), spectra with line amplitudes of up to 4 - 6 have been observed. They still have common features with the spectrum of the iron-precipitate, described in the previous section, but they also exhibit new lines inside the T-range of the precipitation line.

The deep level spectra for sample Fe1150-200-30 are shown in Figure A.1. This Figure shows five DLTS lines and denoted P_1 to P_5 were observed only in this sample, which was annealed for 30 minutes. The peak temperature of lines is independent on the filling pulse durations and at high-temperature sides for the DLTS spectra coincidence. From bandlike criteria, the high temperature peak (P_5) associates the bandlike defects.

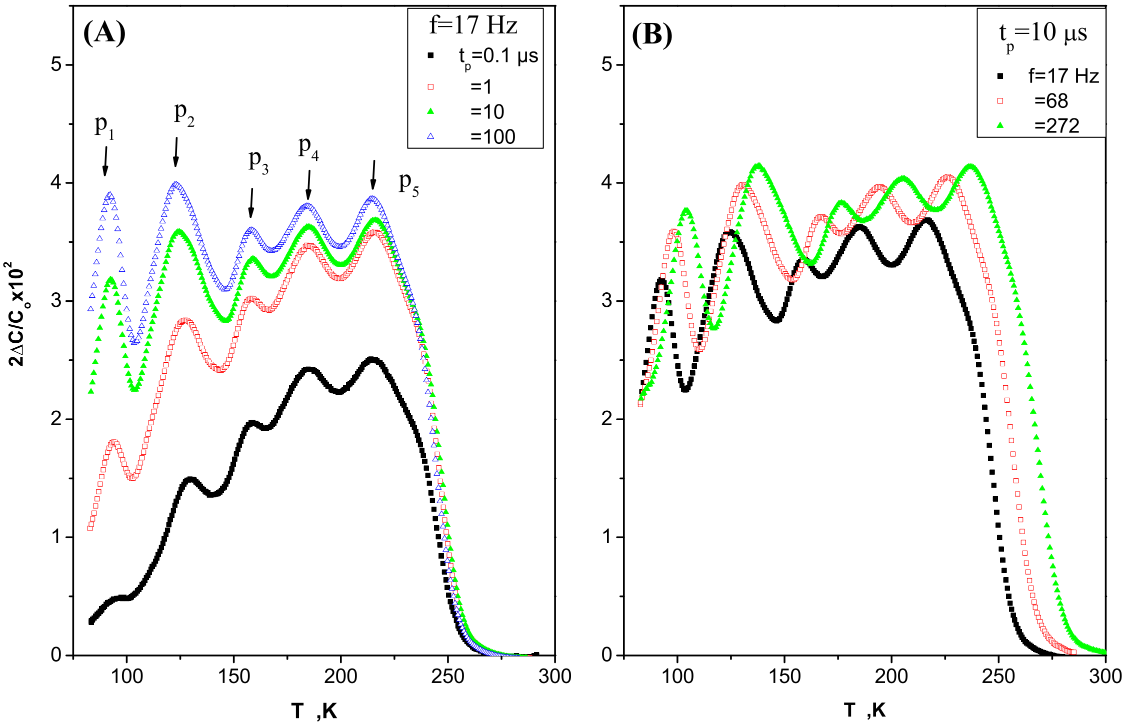

Figure A.1: DLTS spectra for sample Fe1150-200-30. The measurement conditions are (A) Filling pulse duration of 0.1, 1, 10 and 100 μs at frequency $f = 17$ Hz. (B) Repetition frequency of 17, 68 and 272 Hz at filling pulse duration $t_{\mathrm{p}} = 10$ μs. The filling pulse height $U_{\mathrm{p}} = 3$ V and the bias voltage $U_{\mathrm{B}} = 3$ V.

Appendix B

Large amplitude spectra

The DLTS spectra corresponding to annealing at 200 and 250°C for 120 minutes subsequently quench from 1200°C to room temperature in ethylene glycol are shown in Figures B.1 and B.2. The very long anneals reveals drastically in the amplitude and the shape compare to the short and long anneals.

The huge increasing of the amplitude was observed by previous authors in different experiments (nickel silicide[56] and copper silicide[66] in n-type silicon).

DLTS amplitude increases related to the initial case (annealing times 15 and 30 minutes) by factor 4 when the annealing time was changed to 120 minutes. F. Riedel has investigated nickel silicide homogeneity in n-type Si sample by measuring DLTS in different places for one sample. He found that the DLTS line amplitude increased by factor 2 related to the initial case. In addition, the boron-doping concentration in our sample varies from 0.7 to 1×10^{15} cm^{-3} (factor ~ 2), one can say that the factor 4, which appeared with iron precipitations associate to the homogeneity and boron-doping variation factor.

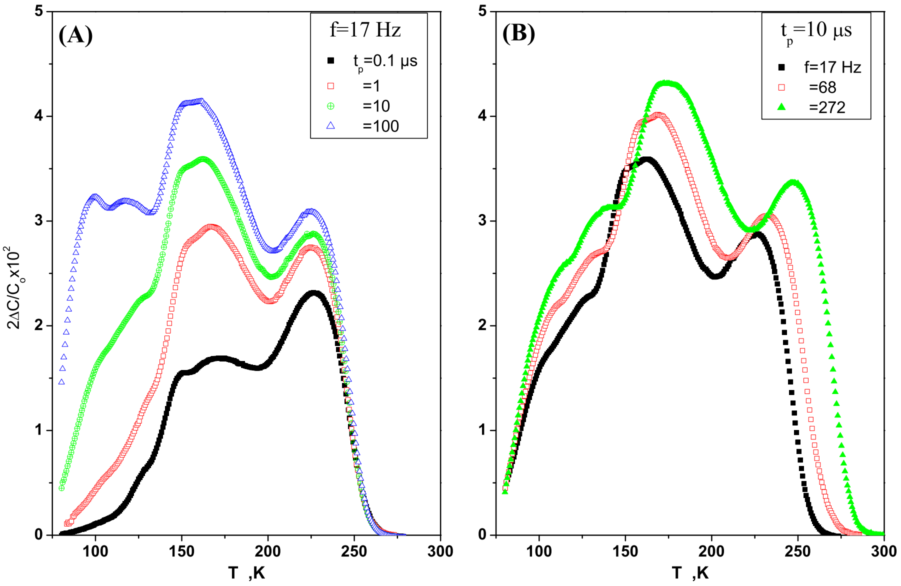

Figure B.1: DLTS spectra for sample Fe1200-200-120. The measurement conditions are (A) Filling pulse duration of 0.1, 1, 10 and 100 μs at frequency $f = 17$ Hz. (B) Repetition frequency of 17, 68 and 272 Hz at filling pulse duration $t_{\rm p} = 10$ μs. The filling pulse height $U_{\rm p} = 3$ V and the bias voltage $U_{\rm B} = 3$ V.

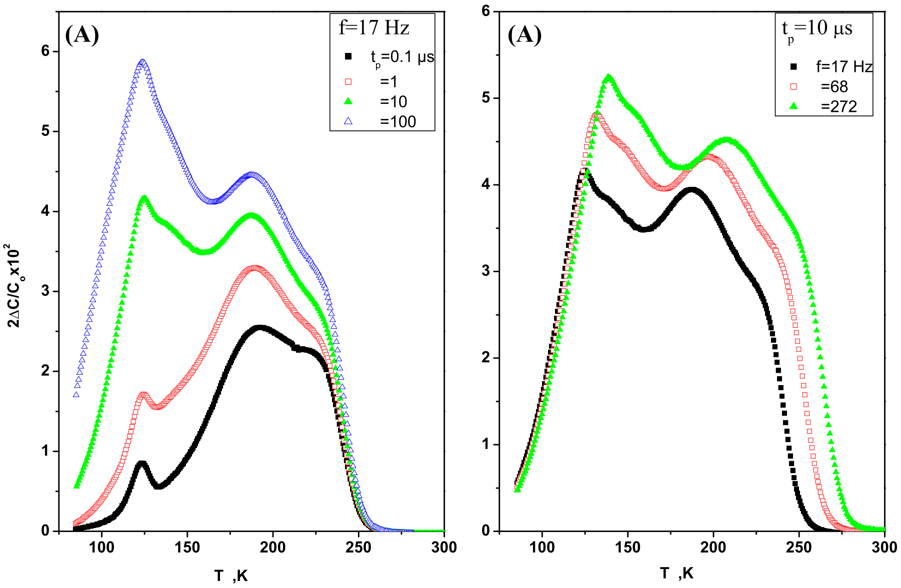

Figure B.2: DLTS spectra for sample Fe1200-250-120. The measurement conditions are (A) Filling pulse duration of 0.1, 1, 10 and 100 μs at frequency $f = 17$ Hz. (B) Repetition frequency of 17, 68 and 272 Hz at filling pulse duration $t_{\rm p} = 10$ μs. The filling pulse height $U_{\rm p} = 3$ V and the bias voltage $U_{\rm B} = 3$ V.

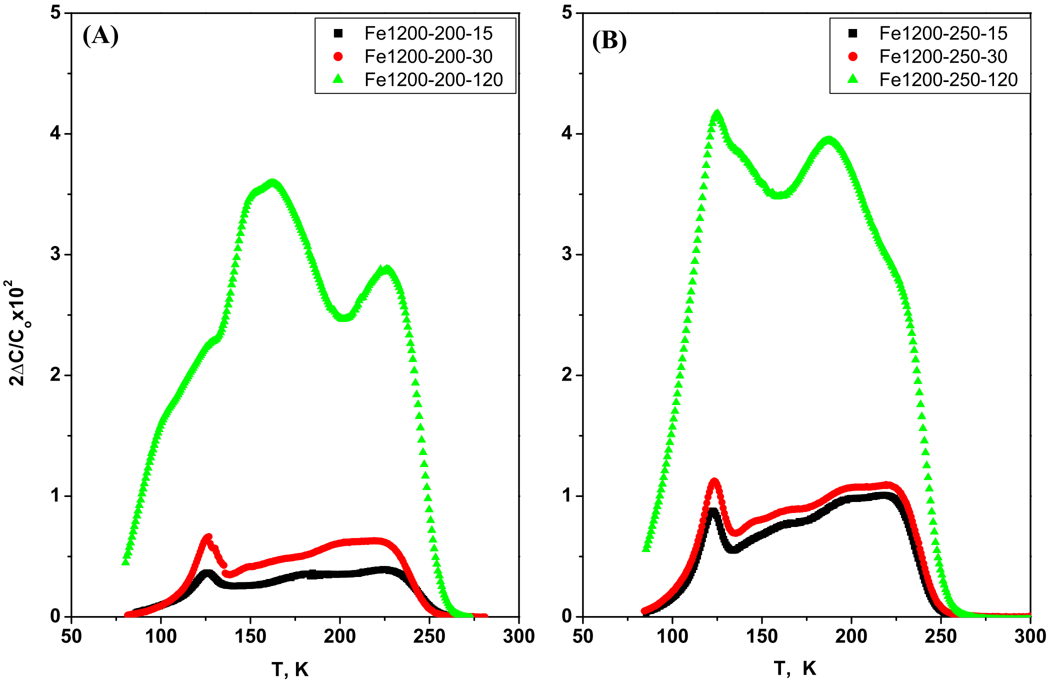

Figure B.3: DLTS spectra after iron-diffused at $T_D = 1200°C$ for 20 min and annealed at $T_A = 250°C$ for different time 15, 30 and 120 minutes. The pulse length $t_p = 1\ \mu s$ and the measuring frequency $f = 17$ Hz. The filling pulse duration $U_p = 3$ V and the bias voltage $U_B = 3$ V.

Bibliography

[1] W. Shockley, IEEE Trans. Electron Devices ED-23 pp. 597–620 (1976).

[2] F. Shimura, *Semiconductor Silicon Crystal Technology* (Academic Press Limited, London, 1988), p. 1.

[3] R. Gleichmann, O. Breitenstein, and U. Mohr, Crystal Res. Technol. **18**, 1115 (1983).

[4] K. Honda, A. Ohsawa, and N. Toyohura, Appl. Phys. Lett. **45**, 270 (1984).

[5] K. Hiramoto, M. Sano, S. Sadamitsu, and N. Fujino, Jpn. J. Appl. Phys., part2 **28**, L2109 (1989).

[6] M. D. Dlamini, Solar Energy Mater. Solar Cells **43**, 353 (1996).

[7] H. S. Reehal, M. P. Lesniak, and A. E. Hughes, J. Phys. D: Appl. Phys. **29**, 934 (1996).

[8] J. H. Reiss, R. R. King, and K. W. Mitchell, Appl. Phys. Lett. **68**, 3302 (1996).

[9] A. A. Istratov, H. Hieslmair, and E. R. Weber, Appl. Phys. A **69**, 13 (1999).

[10] A. A. Istratov, H. Hieslmair, and E. R. Weber, Appl. Phys. A **70**, 489 (2000).

[11] SIA, International technology roadmap for semiconductor, http://www.itrs.net/ntrs/publntrs.nsf, http://www.sematech.org.

[12] J. Wong-Leung, D. J. Eaglesham, J. Sapjeta, D. C. Jacobson, J. M. Poate, and J. S. Williams, J. Appl. Phys. **83**, 580 (1998).

[13] M. Miyazaki, S. Miyazaki, T. Kitamura, T. Aoki, Y. Nakashima, M. Mourai, and T. Shigematsu, Jpn. J. Appl. Phys. **34**, 409 (1995).

[14] E. R. Weber, Appl. Phys. A **30**, 1 (1983).

[15] K. Graff and H. Pieper, J. Electrochem. Soc. **128**, 669 (1981).

[16] S. D. Brotherton, P. Bradley, and A. Gill, J. Appl. Phys. **57**, 1941 (1985).

[17] K. Nakashima, Jpn. J. Appl. Phys. **24**, 785 (1985).

[18] K. Wünstel and P. Wagner, Appl. Phys. A **27**, 207 (1982).

[19] W. Gehlhoff, P. Emanuelsson, P. Omling, and H. G. Grimmeiss, Phys. Rev. B **41**, 8560 (1990).

[20] A. Chantre and L. C. Kimmerling, Mater. Sci. Forum **10-12**, 387 (1986).

[21] S. D. Brotherton, P. Bradley, A. Gill, and E. R. Weber, J. Appl. Phys. **55**, 952 (1984).

[22] H. Lemke, Phys. Status Solidi A **72**, 177 (1982).

[23] R. Czaputa, Appl. Phys. A **49**, 431 (1989).

[24] G. W. Ludwig, Phys. Rev. **137**, A1520 (1965).

[25] N. F. Will, K. Hofmann, and M. Schulz, Appl. Phys. A **41**, 107 (1986).

[26] S. H. Muller, G. M. Tuynman, E. G. Sieverts, and C. A. J. Ammerlaan, Phys. Rev. B **25**, 25 (1982).

[27] C. A. J. Ammerlaan, Solid State Phenom. **6-7**, 591 (1989).

[28] J. J. van Kooten, E. G. Sieverts, and C. A. J. Ammerlaan, Solid State Commun. **64**, 1489 (1987).

[29] W. Gehlhoff, K. Irmscher, and U. Rehse, Mater. Sci. Forum **38-41**, 373 (1989).

[30] A. A. Istratov, H. Hedemann, M. Seibt, O. F. Vyvenko, W. Schröter, T. Heiser, C. Flink, H. Hieslmair, and E. R. Weber, J. Electrochem. Soc. **145**, 3889 (1998).

[31] M. Seibt and W. Schröter, Philos. Mag. A **59**, 337 (1989).

[32] S. Sadamitsu, A. Sasaki, M. Hourai, S. Sumita, and N. Fujino, Jpn. J. Appl. Phys. **30**, 1591 (1991).

[33] N. R. Baldwin and D. G. Ivey, J. Phase Equilibria **16**, 300 (1995).

[34] P. J. Ward, J. Electrochem. Soc. **129**, 2573 (1982).

[35] P. Augustus, Semicond. Int. **8**, 88 (1985).

[36] K. Graff, *Metal Impurities in Silicon-Device Fabrication* (Springer, Berlin, 1995).

[37] M. D. D. Coteau, P. R. Wilshaw, and R. Falster, Solid State Phenom. **19-20**, 27 (1991).

[38] H. Katsumata, Y. Makita, N. Kobayashi, H. Shibata, M. Hasegawa, I. Aksenov, S. Kimura, A. Obara, and S. Uekusa, J. Appl. Phys. **80**, 5955 (1996).

[39] J. Desimoni, F. H. Sanchez, M. B. F. van Raap, H. Bernas, C. Clerc, and X. W. Lin, Phys. Rev. B **51**, 86 (1995).

[40] R. L. Maltez, L. Amaral, M. Behar, A. Vantomme, G. Langouche, and X. W. Lin, Phys. Rev. B **54**, 11659 (1996).

[41] A. G. Cullis and L. E. Katz, Phil. Mag. **30**, 1419 (1974).

[42] M. Seibt and W. Schröter, *Lokalisierung und Identifizierung von Mikrodefekten. Forschungsbericht, Bundesministerium für Forschung und Technologie FRG* (1989).

[43] A. Mesli, T. Heiser, N. Amround, and P. Siffert, Appl. Phys. Lett. **57**, 1898 (1990).

[44] W. Henley and D. A. Ramappa, J. Appl. Phys. **82**, 589 (1997).

[45] D. V. Lang, J. Appl. Phys. **45**, 3023 (1974).

[46] D. V. Lang, J. Appl. Phys. **45**, 3014 (1974).

[47] W. Schröter, J. Kronewitz, U. Gnauert, F. Riedel, and M. Seibt, Phys. Rev. B **52**, 13726 (1995).

[48] O. Engström and A. Alm, J. Appl. Phys. **54**, 5240 (1983).

[49] L. C. Kimmerling and J. R. Patel, Appl. Phys. Lett. **34**, 73 (1979).

[50] P. Omling, E. R. Weber, L. Montelius, H. Alexander, and J. Michel, Phys. Rev. B **32**, 6571 (1985).

[51] T. Figielski, Solid State Electronics **21**, 1403 (1978).

[52] T. Wosinski, *Defect Control in Semiconductors* (North-Holland Publ. Co., 1990), p. 1465.

[53] F. Gelsdorf and W. Schröter, Phil. Mag. A **49**, L35 (1984).

[54] P. N. Grillot, S. A. Ringel, E. A. Fitzgerald, G. P. Watson, and Y. H. Xie, J. Appl. Phys. **77**, 3248 (1995).

[55] H. Hedemann, Ph.D. thesis, Univerität Göttingen (1995).

[56] F. Riedel, Ph.D. thesis, Universität Göttingen (1994).

[57] P. Blood and J. W. Orton, *Techniques of Physics: 14; Electrical Characterization of Semiconductors: Majority Carriers and Electron States* (Academic Press Limited, London, 1992), p. 231.

[58] A. Mircea and A. Mitonneau, Appl. Phys. **8**, 15 (1975).

[59] G. Zoth and W. Bergholz, J. Appl. Phys. **67**, 6764 (1990).

[60] K. Graff and H. Pieper, *Semiconductor Silicon* (Electrochemical Society, Pennigton, NJ, 1981), p. 33.

[61] H. Feichtinger, J. Waltl, and A. Gschwandtner, Solid State Commun. **27**, 867 (1978).

[62] L. C. Kimerling and J. L. Benton, Physica **116B**, 297 (1983).

[63] E. R. Weber, *Properties of Silicon (EMIS Datareviews Series No. 4)* (INSPEC, London, 1988), p. 442.

[64] J. Kronewitz, Ph.D. thesis, Universität Göttingen (1991).

[65] H. Hedemann and W. Schröter, J. Phys. III **7**, 1389 (1997).

[66] A. Sattler, Diploma Thesis, Universität Göttingen (1997).

[67] C. B. Collins and R. O. Carlson, Phys. Rev. **108**, 1409 (1957).

[68] G. W. Ludwig, H. H. Woodbury, and R. O. Carlson, J. Phys. Chem. Solids **8**, 460 (1959).

[69] G. W. Ludwig and H. H. Woodbury, in *Proc. of Int. Conf. on Semiconductor Physics* (Prague, 1960), p. 596.

[70] H. Feichtinger, Inst. Phys. Conf. Ser. **46**, 528 (1979).

[71] K. P. Abdurakhmanov, A. A. Lebedev, J. Kreissl, and S. B. Utamuradova, Sov. Phy. Semicond. **19**, 133 (1985).

[72] J. Wedekind, H. Vollmer, and R. Labusch, Phys. Rev. B **63**, 233202 (2001).

[73] W. Schröter, M. Seibt, and D. Gilles, *Handbook of Semiconductor Technology* (WILEY-VCH Weinheim, 2000), p. 597.

[74] K. A. Mäder, H. von Känel, and A. Baldereschi, Phys. Rev. B **48**, 4364 (1993).

Acknowledgements

I first of all thank Allah who blessed me with this opportunity to conduct this study and endowed knowledge upon me.

I am deeply grateful to Prof. Dr. W. Schröter for his constant support, friendly encouragement and guidance and for digging out papers whenever I asked something. I truly thank him for the interesting discussion and big scientific freedom he always provided, without most of this work would not exist.

I thank Mr. PD. Dr. M. Seibt cordially for the ideas, which contributed very much to the progress of my work, as well as for constant accessibility for questions, and also for the thorough proof-reading of the draft and many useful discussion and comments on it.

Special thanks to Prof. W. Schröter and Prof. H. C. Freyhardt for their kindness of taking the responsibility of being ”Referee” and ”Co-referee” for my thesis.

I thank Prof. Dr. V. Kveder for interesting discussions and many suggestions, which deepened of my understanding of the DLTS technique considerably.

I address my thanks to the members of the group, Dr. F. Riedel, Dr. A. Sattler, Dr. Y. L. Huang, K. Thiel, O. Voss, T. Niermann, C. Rudolf and L. Korte for their valuable help in the experimental work, discussions and for the nice atmosphere they created inside the group.

Dr. K. Ahlborn has often emergency aid for computer problems and helpful partners at the disposal, for this is very cordially thanked to it.

I am grateful to Mr. Ing. M. Schrader, Mr. Frenzel, head of the mechanics workshop, Mr. Langohr, head of the electronic workshop, and all their co-workers for their instant, competent and prompt work.

Ms. N. Feuker and Ms. H. Afshar, are kindly acknowledged for their continuous help with all the small and big administrative problems that a foreigner always has in a foreign country.

My sincere thanks to all the members of the IV. Physical Institute in Göttingen, who always make the working atmosphere quite enjoyable.

I would like to address my sincere gratitude to my wife Asmaa, my daughters Rawda, Marim and Tuka for their never-ending patience, understanding and love.

Finally, my thoughts inevitably go to my parents, my family and to all those persons who always, critically, constructively supported my choices and my work. To them I address my deepest gratitude and the best wishes. I would like to thank and highly appreciate the Egyptian Government for financing my study program.

Göttingen, 2004

– Typeset by $\mathcal{A}\mathcal{M}\mathcal{S}$-TEX–

Lebenslauf

Familienname	Khalil
Vorname	Reda Mahssop El Naby Mohamed
Nationalität	Ägypter
Geburtsdatum	03. Juli, 1967
Geburtsort	Kalubia | Ägypten
Familienstand	verheiratet
Addresse	Christophorusweg 12/415, 37075 Göttingen
1982-1986	Benha Schule Abschluss: Abitur
1986-1990	Aufnahme des Physikstudiums an der Benha Universität
1991-1992	Wehrdienst
März 1996	Diplomprüfung Physik an der Benha Universität
Thema der Masterarbeit	”Effect of Structure Transformation on Electrical Properties of Vanadium Phosphate Glasses”
seit Feb. 2000	Promotion am IV. Physikalischen Institut der Georg-August-Universität Göttingen. Finanzierung der Doktorarbeit durch Stipendium des Landes Ägypten